Chapter 4

Results and discussion

4.1 Sample characterization

Initially, 2PPE measurements were tried out with dye covered TiO_2 surfaces where sample preparation was similar to that for the colloidal films used in the transient absorption spectroscopy. Rutile single crystal samples for TR-2PPE measurements were prepared initially by reducing the crystals at 525 °C in a hydrogen atmosphere for 10 min. This treatment generated sufficient conductivity for electron spectroscopy. These bulk reduced crystals were coated with the dyes by immersing them in the perylene-dye solution. 2PPE spectra of such samples showed a large amount of stationary background signal and UPS measurements revealed relatively large contributions of occupied band gap states. This background made meaningful 2PPE measurements impossible. Therefore, great care was taken in the following experiments to obtain better prepared samples.

4.1.1 Rutile Crystals

A major prerequisite for PES measurements is sufficient bulk conductivity of the sample and satisfactory ohmic contacts. To check for both, a test sample was clamped as usual with two insulated clamps and the liquid alloy InGa was applied to one contact patch only to guarantee an ohmic contact for one clamp. For this sample current-voltage plots were taken. The contact between metal clamp and TiO_2 turned out to be almost ohmic with a resistivity around 2.5 Ω between the two contacts 5 mm apart.

Even newly purchased rutile samples showed occupied band gap states in UPS

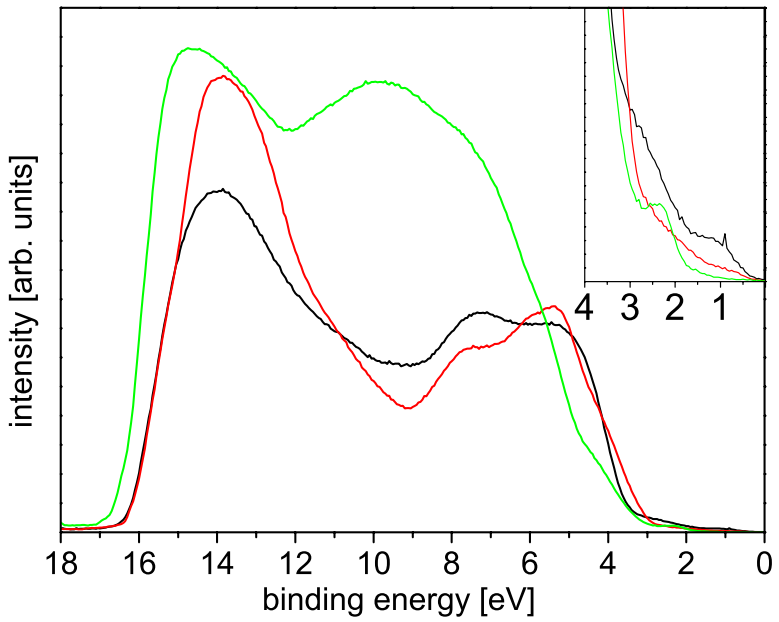

Figure 4.1: UPS spectra of rutile single crystals after heating to 600 °C (black), after 4 cycles of Ar^+ ion bombardment (red) and after coating with a perylene dye (Pe'-tripod) (green)

after heating at 875 K in vacuum, (black curve of Fig. 4.1) [1]. These band gap states could be assigned by XPS measurements to carbon impurities on the surface (black curve Fig. 4.2). The chemical shift of the C 1s peak indicates that these impurities are carbon oxides. Repeated cycles of Ar^+ ion bombardment followed by heating the sample in vacuum reduced the amount of occupied band gap states and also the count rate of the C 1s peak as observed by repeated UPS and XPS measurements. After 4 cycles of sputtering and annealing no carbon could be detected anymore by XPS and further cleaning cycles didn't reduce the signal from band gap states further.

As mentioned in Sec. 2.6.2.1 the preparation of $TiO_2(110)$ rutile surfaces is still under discussion. STM, the method of choice to directly determine the amount of oxygen vacancies on the surface, was not available. Nevertheless, UPS and XPS give the possibility to estimate the stoichiometry of the surface. Reduced crystals are reported to show an occupied Ti 3d peak in the band gap 0.7 eV below the conduction band edge [128, 129] such peak was not observed on surfaces prepared for this work (Fig. 4.1). In addition, the Ti^{4+} and Ti^{3+} peaks are well separated in XPS. No Ti^{3+} contribution could be resolved on crystals prepared with the forementioned method (Fig. 4.3). But, a crystal sputtered with 1000 eV

[1] Heating was necessary because the untreated crystals showed insufficient conductivity for electron spectroscopy.

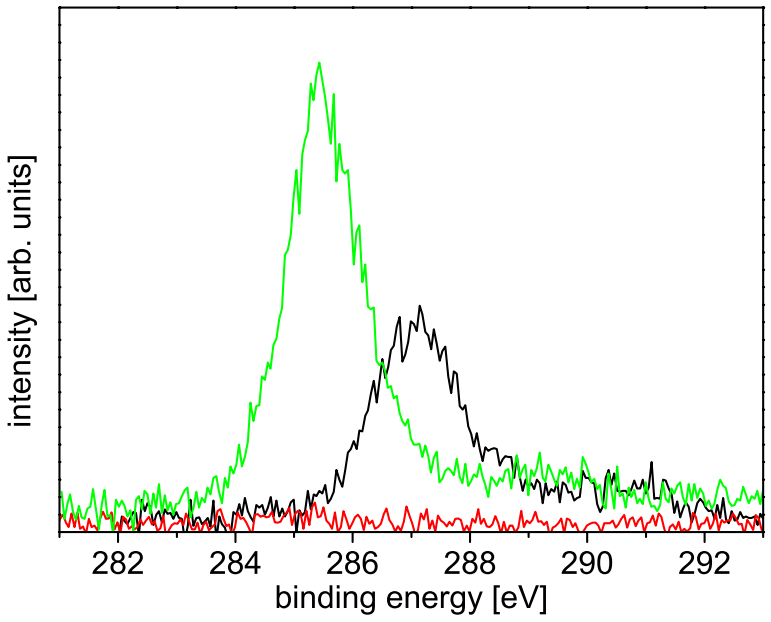

Figure 4.2: XPS C1s spectra of rutile single crystals after heating to 600 °C (black), after 4 cycles of Ar^+ ion bombardment (red) and after coating with perylene (green)

Ar^+ ions for 15 min showed a major contribution from Ti^{3+} (Fig. 4.3).
Moreover, UPS measurements give informations about the work function and the position of the Fermi level. The work function of the bare rutile samples was ranging between 4.4 and 4.7 eV, as deduced from the low energy cutoff of 2PPE. The Fermi level was located 0.1 eV below the conduction band edge assuming a band gap of 3 eV. It should be noted that, in contrast to metal surfaces, the work function of metal oxide surfaces is so surface sensitive that its absolute value is of little significance [97]. The statistical spread over 300 meV should be kept in mind for the following discussions. Another tool for investigating the surface condition is low energy electron diffraction (LEED). LEED measurements of the vacuum annealed surface showed a 1x1 reconstruction with sharp spots indicating a clean well ordered surface. Although cleanliness of the surface is hard to estimate quantitatively from LEED, the 1x1 reconstruction strongly supports a stoichiometric surface since a 1x2 reconstruction has been reported for the reduced surface [128].

4.1.2 Metal single Crystals

The preparation of the low index surfaces of noble metals by sputtering and annealing is a routine technique. As mentioned above, the Cu(111) crystal served

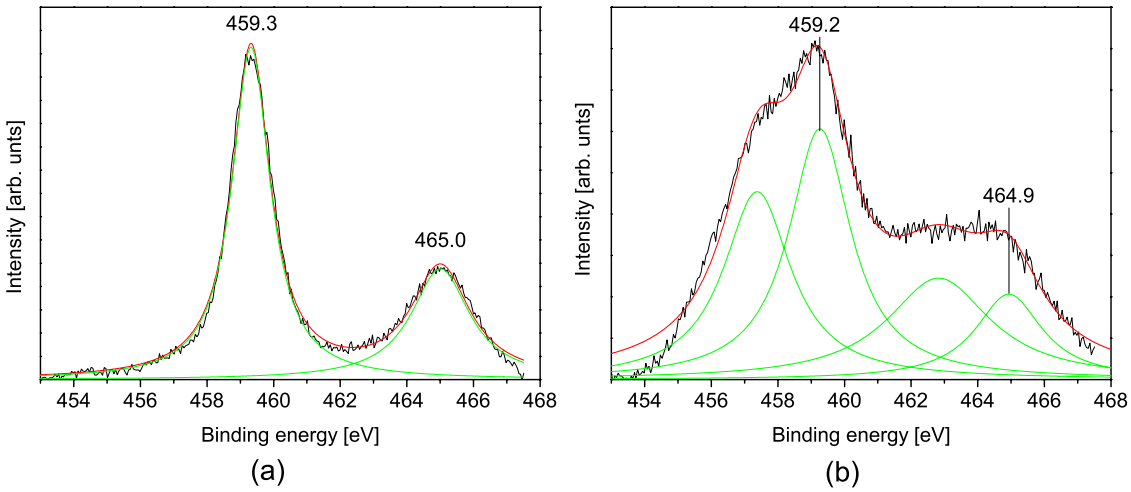

Figure 4.3: XPS Ti 2p spectra of rutile single crystals after 4 cycles of Ar^+ ion bombardment at 700 eV followed by annealing at 875 K (a) and after 15 min 1000 eV Ar^+ ion bombardment without annealing (b). Lorentzian fits (green).

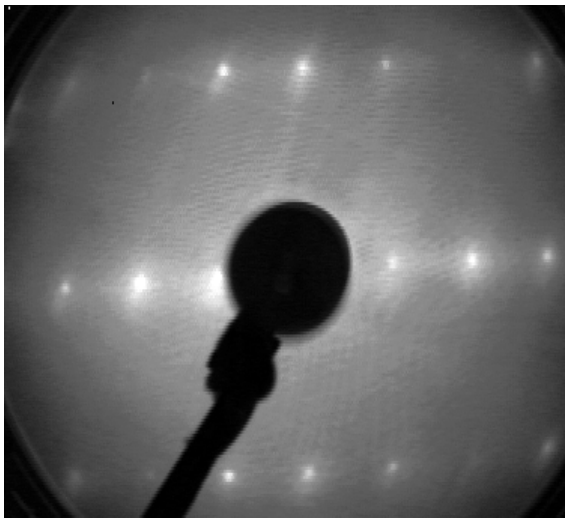

Figure 4.4: LEED pattern of a vacuum annealed TiO_2(110) surface (127 eV).

as a reference sample to measure auto- and crosscorrelation functions. Therefore, cleanliness of the metal samples was only checked by the amplitude and width of the signals from occupied and unoccupied surface states. It is known that surface contamination effectively destroys these states [130, 46]. Accordingly, surface states can be used as indirect indicators for clean surfaces.

4.1.3 Perylene derivatives on TiO_2(110)

4.1.3.1 Level alignment at the interface

All samples were investigated by means of UPS and XPS after the 2PPE measurements had been completed since the adsorbed molecules can be damaged by high energy photons. Again, a mobile UHV chamber was used to transfer the samples to the ESCA chamber.

Fig. 4.5 shows UPS difference spectra of a sample with adsorbed Pe'-tripod and an uncoated reference sample (red). In the lower part an UPS spectrum is shown of the perylene chromophore in gas-phase taken from [131] (black dashed). The black solid line is a convolution of the gas phase spectrum and a Gaussian function with full width at half maximum height of 100 meV. The convolution accounts for the energy resolution of our hemispherical electron energy analyzer as well as possible inhomogeneous broadening. The ionization-potential energy

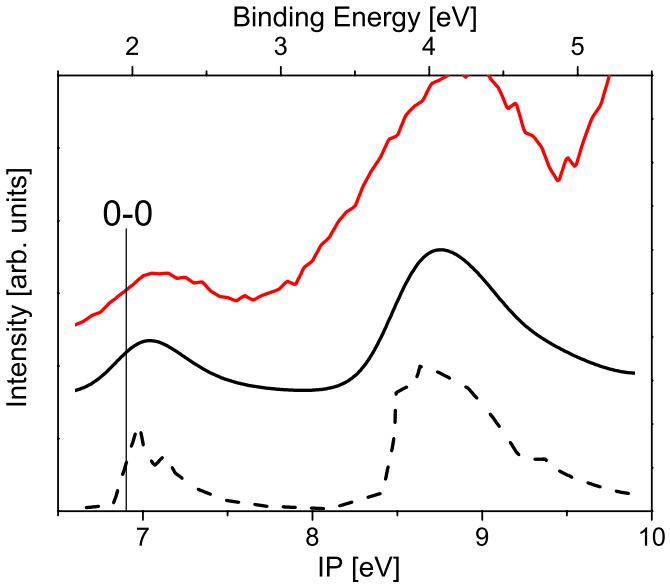

Figure 4.5: UPS difference spectra of the adsorbed Pe'-tripod (red) and UPS spectrum of the perylene chromophore in gas phase (dashed curve) and the latter convoluted with the energy resolution of the energy analyzer (black).

scale of the gas-phase measurement is matched to the vacuum level of the clean TiO_2 rutile surface. The HOMO and HOMO-1 levels are clearly visible. A Gaussian fit of the first peak of the gas-phase spectrum revealed E = 7.08 eV and ΔE = 0.51 eV for position and width of the peak, respectively. For the Pe'-tripod adsorbed on TiO_2 the fit parameters were: E = 7.11 eV and ΔE = 0.84 eV. The 0,0 transition for ionization in the gas phase is located at 6.9 eV (marked in Fig. 4.5) . Thus, the position of the HOMO is shifted by 200 meV against the peak maximum to lower binding energies due to the Franck-Condon progression of the Pe$\rightarrow$Pe$^+$ transition.

The work functions of the samples were measured with the 2PPE apparatus, since energy resolution was much better for 2PPE than UPS and technical problems limited the reliability of the UPS measurements for very low kinetic energy electrons (Sec. 3.2.3). The work functions are given in table 4.1.3.1. The work function was measured independently with both photon energies and different bias voltages of 1 V, 2 V, and 3 V. The work function of the samples changed upon adsorption of the molecules by approximately 0.5 eV.

In addition, Tab. 4.1.3.1 gives the position of the HOMO levels and that of the the excited states of the molecules. The position of the excited state was measured via 2PPE with pump and probe pulses overlapping in time. The photon energies were 2.8 eV and 4.4 eV for the pump and the probe pulse, respectively. Both pulses were p-polarized. A bias voltage between 0 meV and 300 meV was applied between sample and TOF to account for the difference in work function between sample and TOF. The bias had to be kept smaller than the difference in the work functions because the probe pulse had sufficient energy for generating one-photon photoemission that would have covered the 2PPE signal. Therefore, the low energy cutoff of the spectra is determined by the work function of the TOF and not by the density of populated intermediate states. However, it was possible to fit the high energy part of the 2PPE spectra with a Gaussian function after the stationary background had been subtracted when the low energy part was not included in the fit procedure and the full width at half maximum for all fits was fixed at 950 meV. The width of 950 meV for the fit was taken from measurements of some samples where a higher bias voltage was applied. An example of a fitted 2PPE spectrum is given in Fig. 4.6.

For estimating the excited state position from the 2PPE spectra, it has to be taken into account that the excitation as well as the photoemission step introduce a Franck-Condon broadening in the spectrum. The Franck-Condon broadening of the excitation step is dominated by the spectral width of the pump pulse, i.e. 180 meV. The 0,0 transition is located on the low energy side of the energy

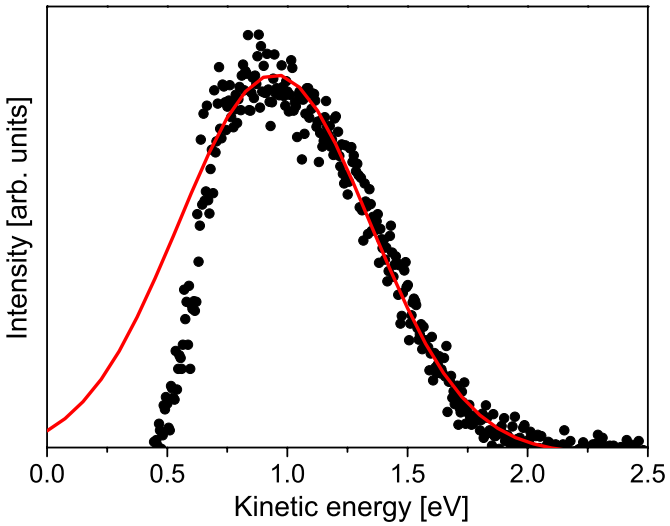

Figure 4.6: 2PPE spectrum of Pe'-CH_2-$PO(OH)_2$ on TiO_2 (black) and a Gaussian fit of the high energy part (red).

distribution.

The photoemission process in 2PPE is comparable to that in UPS discussed above. The width is dominated by the reorganization energy of the $Pe^* \rightarrow Pe^+$ transition and the 0,0 transition is located on the high energy side of the distribution. Thus the pump step leads to a tailing of the energy distribution to higher energies and the probe step leads to a tailing to lower energies. The shift between the maximum of the distribution and the 0,0 transition in the former step can be estimated from the absorption spectrum and the spectrum of the pump pulse and is around 60 meV (Fig. 2.12). The shift for the photoemission step can be estimated from the UPS measurement to be around 200 meV. It should be noted that the latter estimation is not strictly valid as the reactant states in 2PPE and UPS are different. Nevertheless, the excited state position is assumed to be located around 150 meV above the maximum in the 2PPE spectra.

The excited state position given in table 4.1.3.1 was gained by adding the work function of the sample to the measured kinetic energy, subtracting the probe-photon energy and adding the shift of 150 meV, discussed above. The HOMO levels were estimated from the 2PPE measurements by subtracting the S_0-S_1 transition energy (Tab. 2.6.1.1) from the excited state position. The shift of the vacuum level upon adsorption of the molecules is most likely due to the chemical reaction of the molecular acid group with the Ti atoms of the surface and the resulting surface dipole. The dipole potential can be estimated by $-e\,D/2\,\epsilon_0$ [44]. Where D is the surface dipole density [Debye/unit area]. A shift of 0.5 eV of the vacuum level leads to a dipole moment per square nm of 2.65 D. Assuming

Compound name	HOMO position E-E_F[eV] (UPS)	Work function E-E_F [eV] (2PPE)	Excited state pos. E-E_F [eV] (2PPE)	HOMO position E-E_F [eV] (2PPE)
Pe'-COOH	-2.5	3.90	0.44	-2.29
Pe'-CH=CH-COOH	-2.05	4.05	0.51	-2.08
Pe'-CH_2-CH_2-COOH	-2.15	4.05	0.57	-2.17
Pe'-tripod	-2.6	4.20	0.31	-2.27
Pe'-$PO(OH)_2$	-2.6	3.85	0.50	-2.25
Pe'-CH_2-$PO(OH)_2$	-1.85	4.05	0.63	-2.10
Pe'-rod	-2.05	3.70	0.62	-2.07

Table 4.1: Work function and position of HOMO and excited state energy level of the different perylene compounds with respect to the Fermi energy (E_F).

bidentate bridge-like binding (see Sec. 4.1.3.2) one molecule can bind per two surface cells giving 1 molecule per 38.4 Å^2. Taking the dipole moment of formic acid (1.8 D) one ends with a surface coverage of 0.57. Since the actual dipole moment for the bound acid group will certainly differ from that of the free acid group, this value is just a rough estimation.

The differences in the peak positions show no systematic behavior, neither relating to the different anchor groups nor to the length of the spacer group. The variations for the HOMO position extracted from the UPS measurements are larger than that for the positions estimated from 2PPE. One reason is that in UPS the large signal originating from the valence band edge has to be subtracted to extract the peak position. The difference of 310 meV in the excited state positions for the different Pe'-derivatives is not so easily understood. On the one hand the excited state of the directly bound Pe'-COOH is located lower in energy than most of the other Pe' derivatives, on the other hand the Pe'-tripod, the molecule with the longest spacer group, has the lowest excited state position. The ionization potential of the adsorbed molecules ($IP = -E_{HOMO} + E_{work}$) is around 700 meV smaller than that of perylene in gas phase (6.9 eV). This shift is ascribed to screening by the charges in the TiO_2 substrate and the surrounding molecules.

Using 2PPE the work function could be measured with the two different photon energies at hand (e.g. 4.6 eV and 2.8 eV). All samples showed a fast shift of the work function of about 250 meV to lower energies when illuminated with the 4.6 eV UV pulse. This shift took about 10 seconds and was irreversible. The work function measured with 2.8 eV before illumination with the UV light was the same right at the beginning of the shift observed when the UV pulse was present.

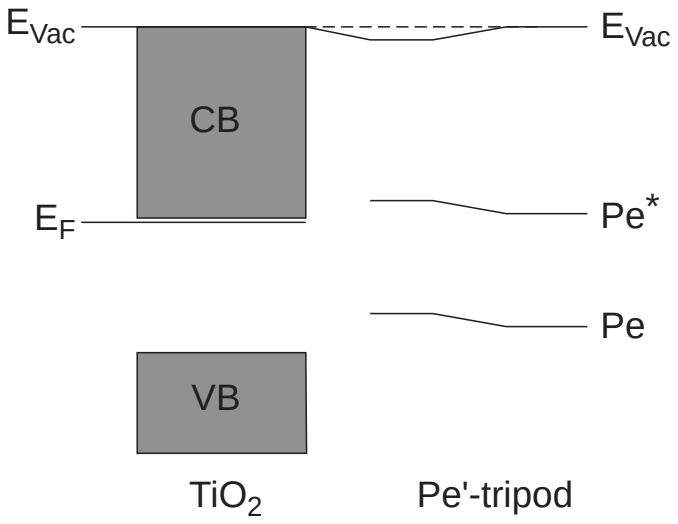

Figure 4.7: Level alignment of Pe'-tripod at the surface of TiO_2. The molecular levels on the right side represent the free molecule, while the molecular levels in the middle represent the aligned levels after adsorption.

Both photon energies resulted in the same work function after illuminating the sample with the UV pulse. As the 2.8 eV pulse had ten times the intensity of the 4.6 eV pulse a thermal reaction can be excluded. This behavior indicates a photo-driven reaction on the sample surface. One scenario would be, that the acid group binds at first just with one oxygen atom to a titanium atom and forms a hydrogen bond with a neighboring oxygen atom. This conformation is reported for formic acid on rutile (111) [105] and carboxylic acid on anatase surfaces [106]. The reason for the monodentate bonding may be the presence of methanol in the solution (Sec. 2.6.2.1). The dissociation of hydrogen and the bond formation of the second oxygen atom to a titanium atom may be a photo-driven process. For all further measurements it was checked that the shift in work function was finished prior to the measurement.

4.1.3.2 Binding geometry

Polarization dependence As mentioned in Sec. 2.6.1.1 the S_0-S_1 transition dipole moment of perylene is oriented along the long molecular axis. With this knowledge at hand one can measure the orientation of the perylene with respect to the TiO_2 surface by varying the polarization and/or the angle of incidence of the pulses, provided the molecules form an ordered layer on the surface. In addition the rutile (110) surface has a characteristic anisotropic surface structure with rows of oxygen along the [001] direction (Sec. 2.16). This anisotropy may

result in the alignment of the adsorbed molecules along these rows. To account for this anisotropy, two samples mounted with the [001] axis perpendicular to each other were measured to check for the binding geometry. The angle of incidence for the light pulses was 45° when the electron emission was measured in surface normal direction. Changing the angle of incidence was only possible by rotating the sample. Thus, the emission angle for photo-electrons changed simultaneously.

First polarization-dependent measurements were done for the Pe'-tripod:TiO_2 system. Because of the rigid bridge and the three acid groups it was expected that the long molecular axis should be oriented normal to the surface was expected, due to the large distance between the acid groups an alignment of the molecular plane along the [001] oxygen rows was not expected. Fig. 4.8 shows 2PPE kinetic energy spectra of Pe'-tripod at t_0 with p-polarized (red) and s-polarized (black) pump pulses (2.8 eV). The monochromatic background generated by both pulses is subtracted in Fig. 4.8. Changing the polarization of the probe pulse (4.6 eV) had no effect except for a small loss of signal amplitude because of the polarization dependent reflection of the signal. Time-resolved 2PPE measurements were done at different angles, but no angular dependence of the TR-2PPE signal could be observed within a range of ±30° with respect to the surface normal direction. Thus it was concluded that Pe'-tripod binds predominantly in an upright position (Fig. 4.9.a) and photoemission is not sharply directed.

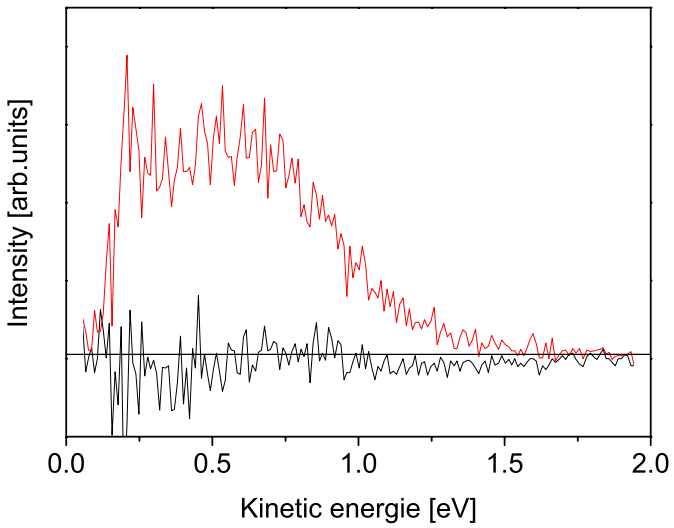

Figure 4.8: 2PPE kinetic energy spectra of Pe'-tripod at t_0 with the pump pulse p-polarized (red) and s-polarized (black). The time independent background was subtracted from both spectra

Polarization dependent measurements of the other Pe'-bridge-carboxylic-acid:TiO_2 systems yielded the expected results. For Pe'-CH=CH-COOH on rutile the long molecular axis of perylene was oriented perpendicular to the surface. This supports a bridge like bonding of the two acid oxygen atoms to two five-fold coordinated, neighboring Ti atoms along the [001] direction (cf. discussion in Sec. 2.6.2.1) and the trans-conformation of the double bond. This agrees with semi-empirical PM3 calculations predicting a slightly lower total energy (25 kJ/mol) for trans-Pe'-CH=CH-COOH [64] than for the cis-configuration. In addition, in cis-configuration the molecule could hardly bind on the surface for sterical reasons (Fig. 4.9.b). It should be mentioned that the orientation of the short molecular axis of perylene with respect to the crystal axis could not be determined.
In contrast, no polarization dependence could be measured for the Pe'-CH_2-CH_2-COOH:TiO_2 system. This agrees with the rotational degree of freedom in the single bond between the two methylene groups. A preferential orientation of the perylene chromophore with respect to the TiO_2 surface is not expected (Fig. 4.9.c). For the Pe'-COOH:TiO_2 system again an upright binding geometry was found, as expected. Because of the short distance the interaction of the perylene chromophore with the oxygen rows of the rutile surface should be much stronger in this system and it is likely that the molecular planes are arranged along [001] direction [108]. But to the best of my knowledge the transition dipole moment from the excited molecular state to free electron states is not known for perylene. From orbital calculations [62] it can be gathered that the transition dipole is parallel to the short molecular axis and thus for an obtuse angle of incidence the probe pulse should exhibit polarization dependence. However, this could not be observed.

Angular dependence A series of 2PPE spectra with p- and s-polarized pump pulses at different angles were measured for the Pe'-CH=CH-COOH:TiO_2 system to elucidate further the photoemission yield in dependence on the emission angle. Fig. 4.10 shows the geometry for angle resolved 2PPE. As mentioned above, the emission angle changed simultaneously with the angle of incidence. Another disadvantage of the setup was that the sample surface was not in plane with the rotation axis and the measured spot of the sample changed with the rotation angle. Therefore, for every value of the angle spectra with p- and s-polarized pump pulses were measured. It was checked that the pulse intensity at the entrance window of the UHV chamber didn't change with polarization. Assuming that

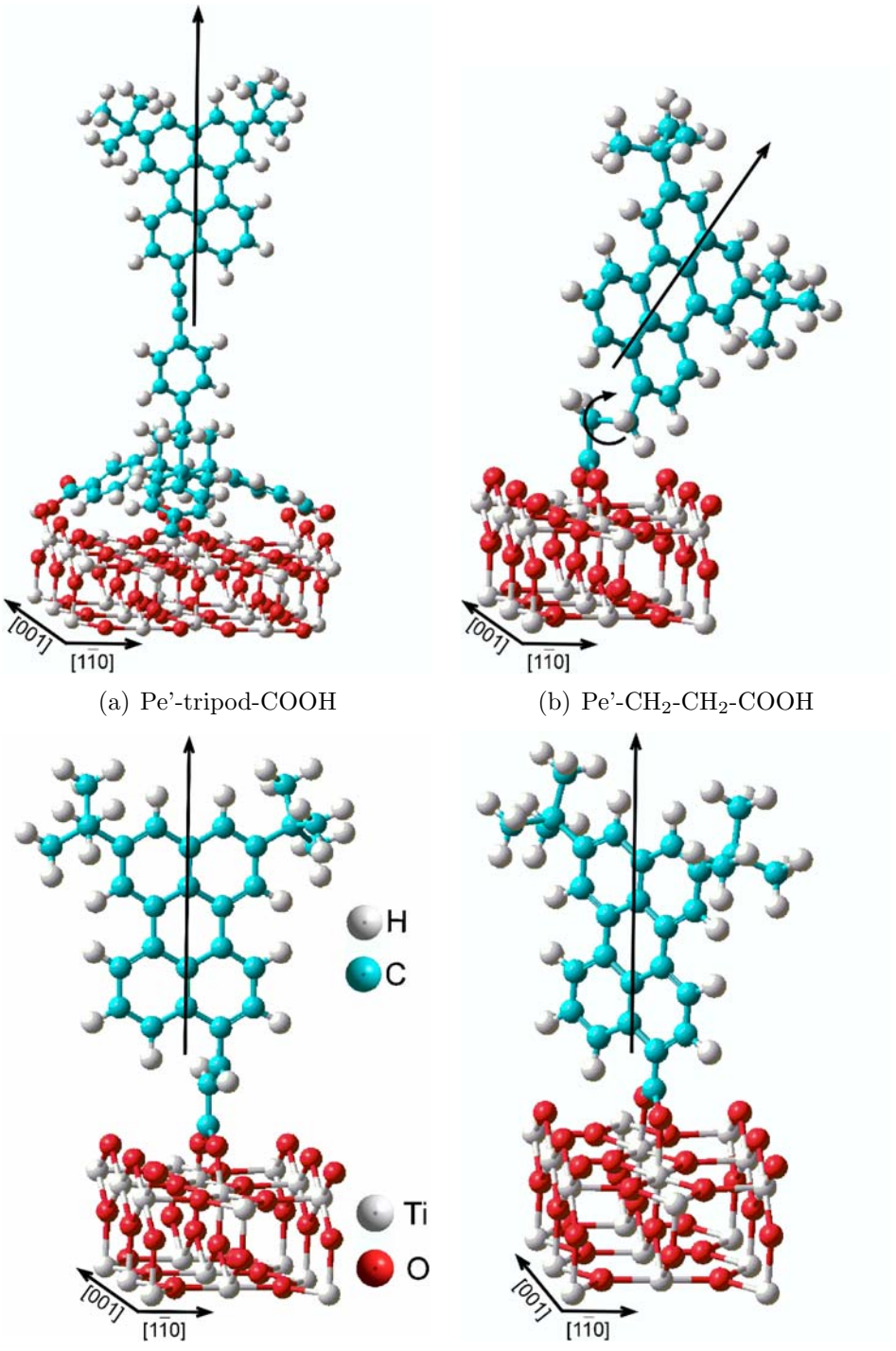

(a) Pe'-tripod-COOH

(b) Pe'-CH_2-CH_2-COOH

(c) Pe'-CH=CH-COOH

(d) Pe'-COOH

Figure 4.9: Balls and sticks models of the different adsorption geometries of perylene derivatives on TiO_2 as deduced from polarization dependent measurements. The binding geometry of Pe'-CH_2-CH_2-COOH is undefined because of the rotational degree of freedom in the single bond between the two methylene groups.

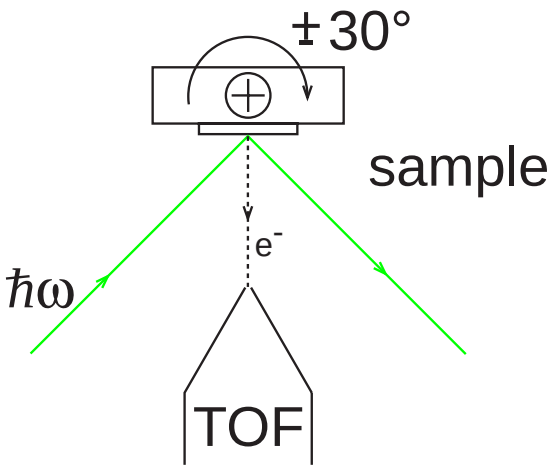

Figure 4.10: Diagram of the experimental setup for angular resolved 2PPE measurements.

any background signal is isotropic with respect to the polarization, the difference between s- and p-polarized spectra only contains signal from the ordered organic layer. This procedure was used to reduce deviations in the peak height between spectra at different angles stemming from the use of different spots on the sample.

The photoemission yield W is proportional to the square of the projection of the electromagnetic field vector at the surface for the pump pulse $\boldsymbol{E}^{pump}$ onto the S_0-S_1 transition dipole moment of the perylene $\boldsymbol{\mu}^{ex}$ multiplied by the probe field $\boldsymbol{E}^{probe}$ projected onto the transition dipole moment for photoionization $\boldsymbol{\mu}^{ion}$. This reads

$$W \propto |\boldsymbol{E}^{pump} \cdot \boldsymbol{\mu}^{ex}|^2 \, |\boldsymbol{E}^{probe} \cdot \boldsymbol{\mu}^{ion}|^2 \, . \tag{4.1.1}$$

The $\vec{E}$-field on the vacuum side at the surface if given by [132, 133]:

$$E_y^i = \left(1 - \frac{\sqrt{\epsilon_i - \sin^2(\Theta)} - \cos(\Theta)}{\sqrt{\epsilon_i - \sin^2(\Theta)} + \cos(\Theta)}\right) E_0 \tag{4.1.2}$$

for s-polarized light,

$$E_x^i = \left(1 - \frac{\epsilon_i \cos(\Theta) - \sqrt{\epsilon_i - \sin^2(\Theta)}}{\epsilon_i \cos(\Theta) + \sqrt{\epsilon_i - \sin^2(\Theta)}}\right) E_0 \cos(\Theta) \tag{4.1.3}$$

, and

$$E_z^i = \left(1 + \frac{\epsilon_i \cos(\Theta) - \sqrt{\epsilon_i - \sin^2(\Theta)}}{\epsilon_i \cos(\Theta) + \sqrt{\epsilon_i - \sin^2(\Theta)}}\right) E_0 \sin(\Theta) \tag{4.1.4}$$

for p-polarized light.
Directions and angles are defined in Fig. 4.11. $i = pump, probe$ accounts for the field of the pump and the probe pulse, respectively, and ϵ_i is the dielectric constant. For a molecule bound perpendicular to the surface – like Pe'-CH=CH-COOH – only μ_z^{ex} is non-zero. The direction of $\boldsymbol{\mu}^{ion}$ with respect to the chromophore is not known. Assuming, that the chromophore can rotate freely around the long molecular axis, the dipole moments for the photoionization step are randomly distributed in the x-y plane. For this case it has been shown that the transition probability is given by [134]:

$$W^{ion} \propto 0.5\,(\mu_0^{ion})^2\,\sin^2\Psi|E_x^{probe}|^2 + (\mu_0^{ion})^2\,\cos^2\Psi|E_y^{probe}|^2 \tag{4.1.5}$$

Where Ψ is the angle between the dipole moment and the z-axis. The difference spectra of p-pol pump, p-pol probe and s-pol pump, p-pol probe fulfill:

$$W \propto |E_z^{pump}\mu_z^{ex}|^2 * W^{ion} \tag{4.1.6}$$

Where μ_z^{ex} is the transition dipole moment for the excitation step.
Fig. 4.12 shows the peak height of the 2PPE difference signal at t_0 between p- and s-polarized pump pulses as a function of the angle of incidence (dots), the probe pulse was kept p-polarized. The peak height was gathered from Lorentzian fits of the difference spectra. Fig. 4.12(a) shows a measurement with the plane of incidence perpendicular to [001], i.e. perpendicular to the oxygen rows on the surface. Fig. 4.12(b) shows a measurement with the plane of incidence parallel to [001]. The red curves are plots of equation 4.1.6 where E_0 was adjusted to reproduce the absolute intensity, Ψ was adjusted to reproduce the shape and

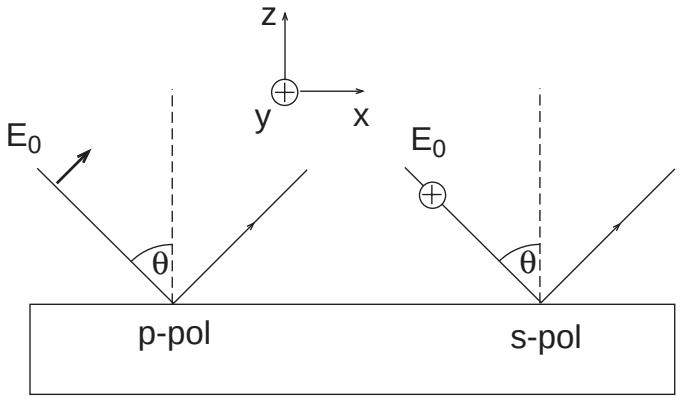

Figure 4.11: Schematic representation of a plane, linear polarized wave incident at an angle Θ.

$\mu_0^{ex} = \mu_0^{ion} = 1$. The dielectric response of TiO_2 is taken from the literature: $\epsilon_{pump} = (3.14)^2$ (2.8 eV), $\epsilon_{probe} = (3.3 + i3.5)^2$ (4.4 eV) [135]. For the best fit the

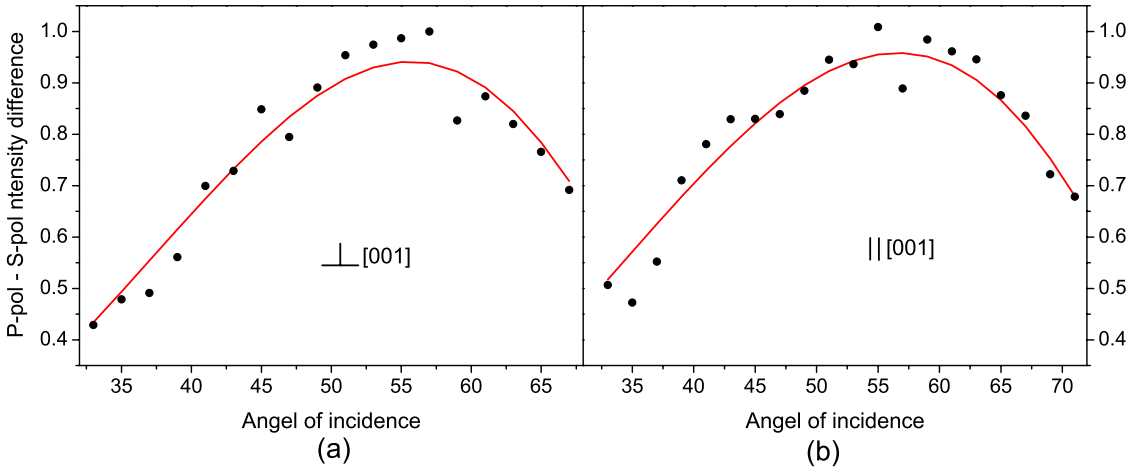

Figure 4.12: Peak height of the 2PPE difference signal between p- and s-polarized pump pulse as a function of the angle of incidence (black) for Pe'-CH=CH-COOH on rutile measured with the plane of incidence perpendicular (a) and parallel (b) to [001]. Plot of equation 4.1.6 (red).

angle between the transition dipole moment for the photoionization step and the long axis of the chromophore is $\Psi = 87°$ and $\Psi = 84°$ for the plane of incidence perpendicular and parallel to the [001] direction, respectively. The deviation for both the samples is believed to be due to the error in the measurement introduced by the simultaneous shift of the light spot position with the change of the angle and due to the small number of measured values. The transition dipole moment for the photoionization step is located on a cone with opening angle around 85° and symmetry axis normal to the surface and shows that no alignment of the molecular plane parallel to the surface is observed. The polarization dependent electron yield is obviously well described by Eq. 4.1.6 for both orientations of the crystal (Fig. 4.12). Therefore, it is concluded that photoemission from the first excited state of the perylene chromophore on the surface of TiO_2 is nearly isotropic.

Polarization dependent and angular resolved 2PPE turned out to be an excellent tool to determine the binding geometry of adsorbed molecules. The same measurements described above for Pe'-CH=CH-COOH were performed for the Pe'-rod molecule bound via one phosphonic acid group to TiO_2. For this molecule the p-pol - s-pol difference in peak height turned out to be very different for the two different oriented crystals (Fig. 4.14). When the plane of incidence is parallel to the [001] direction the difference becomes even negative. Thus, it is assumed

that the molecule is tilted with respect to the surface normal. Now both transition dipole moments (excitation and ionization) have to be projected onto the $\vec{E}$-field with the plane of incidence lying in the x-z plane. Angles and directions are given in Fig. 4.13. For the excitation dipole moment the projection reads:

$$\begin{aligned} \mu_x^{ex} &= \mu_0^{ex} \sin\alpha_1 \cos\alpha_2 \\ \mu_y^{ex} &= \mu_0^{ex} \sin\alpha_1 \sin\alpha_2 \\ \mu_z^{ex} &= \mu_0^{ex} \cos\alpha_1 \ , \end{aligned} \tag{4.1.7}$$

and for the ionization dipole moment in the molecular coordinate system $\tilde{r} = [\tilde{x}, \tilde{y}, \tilde{z}]$:

$$\begin{aligned} \mu_{\tilde{x}}^{ion} &= \mu_0^{ion} \sin\beta_1 \cos\beta_2 \\ \mu_{\tilde{y}}^{ion} &= \mu_0^{ion} \sin\beta_1 \sin\beta_2 \\ \mu_{\tilde{z}}^{ion} &= \mu_0^{ion} \cos\beta_1 \ . \end{aligned} \tag{4.1.8}$$

The transformation in the coordinate system of the $\vec{E}$-field is given by:

$$\vec{\mu}^{ion} = D_z(\alpha_2) D_y(\alpha_1) \tilde{r} \ . \tag{4.1.9}$$

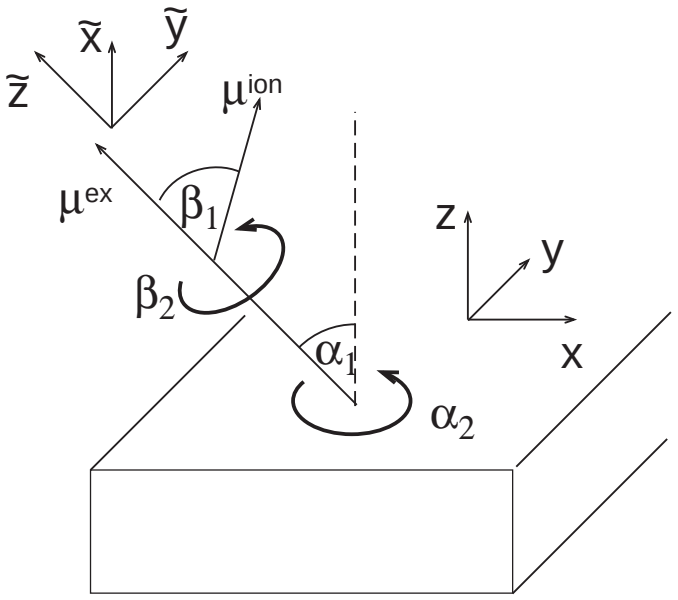

Figure 4.13: Coordinate systems used for Eq. 4.1.10. $[x, y, z]$ is fixed with respect to the $\vec{E}$-field and $[\tilde{x}, \tilde{y}, \tilde{z}]$ is fixed with respect to the long molecular axis.

Where D are the usual rotation matrices. The difference in the photoemission yield W between p- and s-polarized pump pulse (1st term) and p-polarized probe pulse (2nd term) is proportional to:

$$W \propto \left(\left| E_x^{pump}\, \mu_x^{ex} + E_z^{pump}\, \mu_z^{ex} \right|^2 - \left| E_y^{pump}\, \mu_y^{ex} \right|^2 \right) \times \left(\left| E_x^{probe}\, \mu_x^{ion} + E_z^{probe}\, \mu_z^{ion} \right|^2 \right) \tag{4.1.10}$$

Eq. 4.1.10 is valid for both sample orientations, just α_2 will differ by $+\pi/2$ for the plane of incidence being parallel to [001]. In principle, an integration over β_2 would have to be performed to account for the rotational degree of freedom around the long molecular axis. However, it is not clear whether the transition dipole for photoemission is randomly distributed around the long molecular axis. Instead of integrating over β_2, β_2 will be allowed to vary in the fitting procedure.

Fig. 4.14 shows the polarization dependent electron yield as a function of the

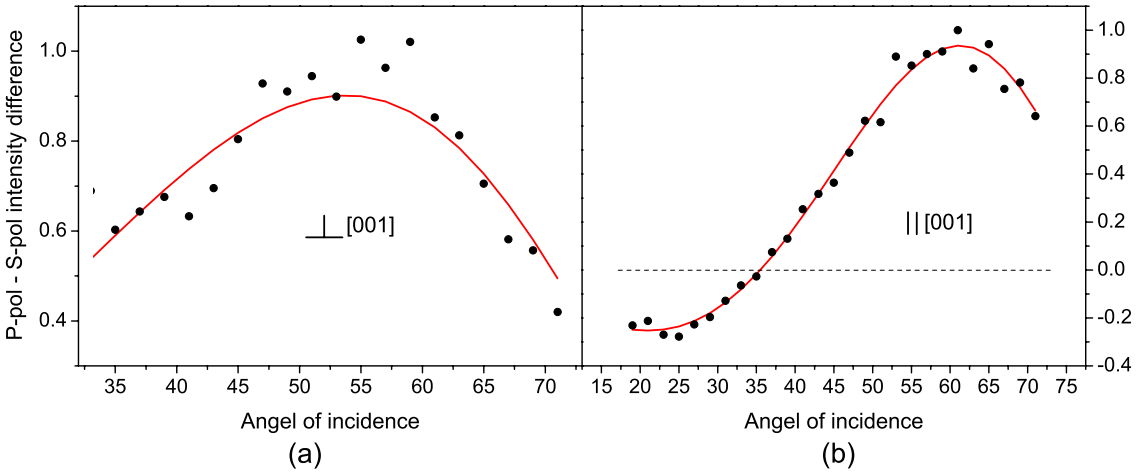

Figure 4.14: Peak height of the 2PPE difference signal between p- and s-polarized pump pulse as a function of the angle of incidence for Pe'-rod on rutile (black), measured with the plane of incidence perpendicular (a) and parallel (b) to [001]. Plot of equation 4.1.10 (red).

angle of incidence for the Pe'-rod adsorbed on the rutile surface (dots) with the plane of incidence perpendicular (a) and parallel (b) to the [001] axis. Red lines

are solutions of equation 4.1.10. The parameters for the perpendicular case are:

$$\begin{aligned} \alpha_1 &= 80^\circ \\ \alpha_2 &= 8^\circ \\ \beta_1 &= 85^\circ \text{ fixed} \\ \beta_2 &= 4^\circ \ , \end{aligned}$$

and for the parallel case:

$$\begin{aligned} \alpha_1 &= 58^\circ \\ \alpha_2 &= 118^\circ \\ \beta_1 &= 85^\circ \text{ fixed} \\ \beta_2 &= 52^\circ \ . \end{aligned}$$

It should be mentioned that, because of the lack of knowledge concerning the exact direction of the transition dipole moment for the ionization step with respect to the main axis of the molecule and the alignment of the molecular plane with respect to the surface, the rotation angle β_2 of the ionization dipole moment is not well defined. The tilt angle β_1 was fixed during the fitting procedure. However, for the sample with the plane of incidence parallel to [001] the tilt angle α_1 of the long molecular axis with respect to the surface normal is quite reliable because the pole of Eq. 4.1.10 depends only on the excitation step. To illustrate this point, Eq. 4.1.10 is plotted in Fig. 4.15 with α_1 fixed to 56°, 58° and 60°. α_2 and β_2 were allowed to vary. The difference of α_2 between both samples of 110° accounts for the alignment of both the samples with the [001] direction of one sample being perpendicular to the [001] direction of the other sample.

From the angular-resolved measurement the bonding geometry of the Pe'-rod bound via a phosphonic acid group to the TiO_2 rutile (110) surface could be deduced. The long molecular axis is tilted against [110] with an angle of around 58° in the direction perpendicular to the oxygen rows. This configuration is compatible with a bi- as well as a monodentade binding geometry with one or two hydrogen bonds, respectively (cf. Sec. 2.6.2.1). A balls and sticks model for the Pe'-rod bound with a bidentate configuration onto the TiO_2 surface is shown in Fig. 4.16.

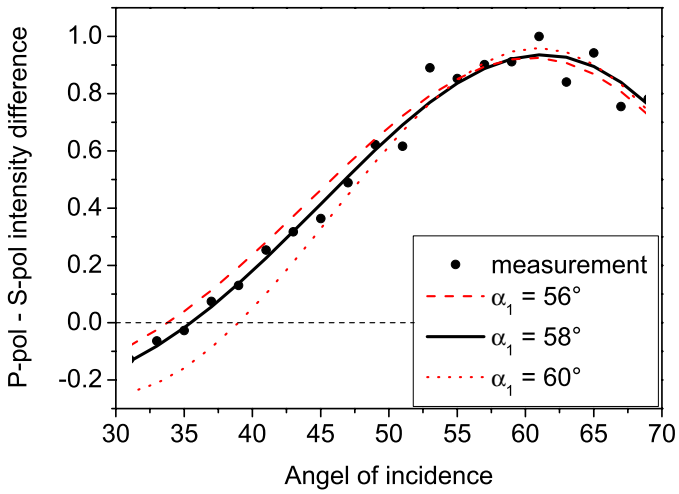

Figure 4.15: Plot of equation 4.1.10 for three different tilt angles α_1 and the measurement with the plane of incidence parallel to [001] (dots).

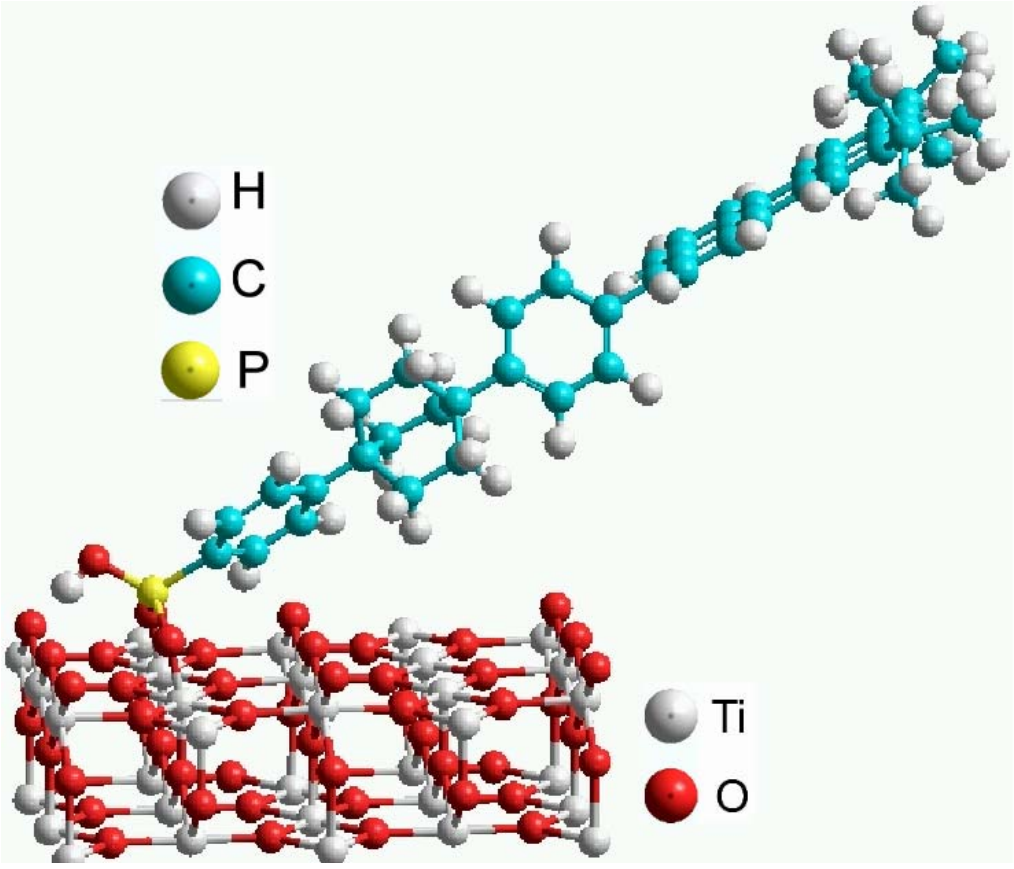

Figure 4.16: Balls and sticks model of the adsorption geometries of Pe'-rod on TiO_2 rutile as deduced from angular resolved measurements.

4.2 Time-dependent 2PPE signals of the bare surfaces

To distinguish between adsorbate induced and substrate induced contributions to the 2PPE signals it is important to establish first the TR-2PPE spectra of the bare surfaces. For silver single crystals these data are available. The exceptionally good time resolution of the presented 2PPE setup allowed, however, the time resolved measurement of the lifetimes of image potential states on Ag and Cu(111) surfaces. For the first time the lifetimes could be extracted from the falling edges of the crosscorrelations. These data are published in Appl. Phys. B [136]. TR-2PPE spectra were measured for the Ag(110) surface for comparison with the Pe'-thiol:Ag(110) system discussed in Sec. 4.3.2.
In principle the rutile TiO_2(110) surface should not give any 2PPE signal when the pump pulse has less then 3 eV energy. But due to the presence of occupied gap states, even at pump photon energies of 2.8 eV a weak 2PPE signal is measured. To illucidate the dynamics of inter-band excited electrons in the conduction-band of TiO_2 pump energies of 3.2 eV were used in addition.

4.2.1 TR-2PPE on bare Ag and Cu single crystal surfaces

The performance of the modified laser system (3.1) was tested by measuring the lifetime of image potential states on Cu(111) and Ag(111) surfaces. In addition the transient 2PPE signal of the bare Ag(110) surface was measured to obtain a reference for the adsorbate covered surface.

4.2.1.1 Cu(111)

The relevant energy levels together with the 2PPE process for Cu(111) are shown in Fig. 4.17. The n=1 IS can be populated from the occupied n=0 SS either directly when the pump wavelength is in resonance with the transition frequency or indirectly by quasi-elastic scattering of electrons with $K_{||} \neq 0$ when the pump wavelength is off resonance with the SS-IS transition [113]. In the latter case the 2PPE spectrum shows two peaks, one representing resonant excitation of the image potential state, the other nonresonant 2PPE from the occupied surface state. As the intermediate state in the latter process is virtual, TR-2PPE reproduces the crosscorrelation trace of the pulses. Thus it is possible to measure t_0 and the CC trace simultaneously with the temporal evolution of the IS.

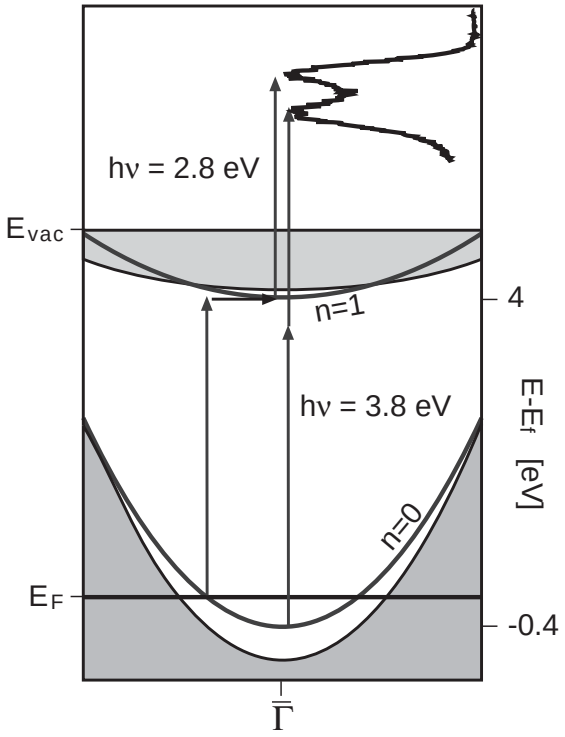

Figure 4.17: Surface projected bulk band structure and dispersion of the n=0 surface state and n=1 image potential state together with the TR-2PPE scheme for the Cu(111) surface. Effective electron masses and binding energies taken from [137].

For obtaining well separated surface- and image potential state contributions in the spectra, the pump wavelength was tuned to 325 nm (3.8 eV). The probe wavelength was 435 nm (2.8 eV). The pulse energies were 0.1 nJ and 0.2 nJ for pump and probe pulse, respectively. Fig. 4.18 shows transients for the image potential- and surface state together with fitted curves. The AC trace (20 fs pulse) of the 325 nm pulse was taken from the high energy part of TR-2PPE on a polycrystalline gold sample.

Fits for both transients were performed using Eq. 2.4.7. The photoemission step was considered by convoluting the intermediate state population with the probe pulse. The SS was fitted with a detuning of $\delta = 400$ meV between resonance and laser frequency to determine t_0 and the width of the pump pulse. With these values at hand, the dephasing and decay rates for the IS were obtained by fitting the transient with the same model assuming resonant excitation (Fig. 4.18). This gives a lifetime of $T_1 = 12 \pm 2$ fs and a dephasing time of sub-1 fs. The very fast dephasing is attributed to a poor surface order connected with the history of the sample. The sample was routinely used for pulse-correlation measurements and treated with cycles of ion bombardment and heating as a daily

routine. In quantum-beat experiments it has been shown that surface defects strongly influence the dephasing time whereas the lifetime changes only slightly [138]. Nevertheless, decay rates are affected by the surface quality [46] and the reported lifetimes should be taken with care. Due to the very fast dephasing the difference between the Bloch model and rate equations is negligible. Thus fitting with a rate model gives the same lifetime.

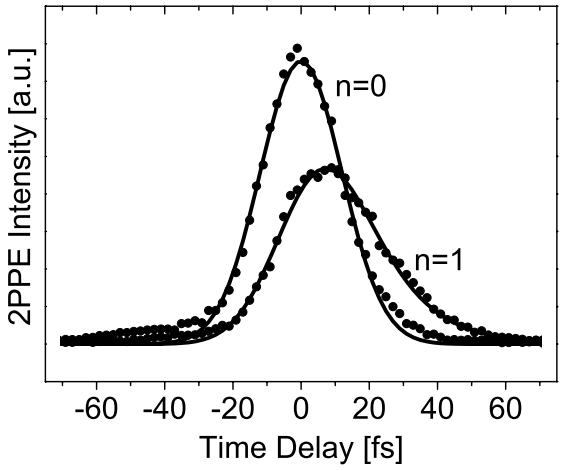

Figure 4.18: Transients for the n=0 surface state and n=1 image potential state at Cu(111) together with the fitted curves obtained from the Bloch model.

4.2.1.2 Ag(111)

The band structures of copper (Fig.4.17) and silver (Fig.4.19) surfaces are quite similar. But due to the higher lying n=0 surface state and the lower work function, it is possible to resonantly populate the n=2 IS [140] and thus strongly enhance its emission[2]. With a pump pulse tuned in resonance with the n=0 - n=2 transition (280 nm) the TR-2PPE spectra show two peaks. One at higher energies originating from the resonant process and another for the n=1 IS populated non-resonantly from states below the Fermi level. In contrast to the measurement on Cu(111) it is not possible to measure the crosscorrelation trace and t_0 simultaneously with the lifetimes of the image potential state under these conditions. Therefore, the CC trace and t_0 were obtained from the TR-2PPE signal of highly excited electrons in a polycrystalline gold sample prior to the measurement on Ag ($CC_{280+435}$=33 fs $FWHM_{Gauss}$).
The data analysis was identical to that described for Cu(111). The pulse width

[2]The resonance energy for the n=2 IS on Cu(111) is hν=5.1 eV

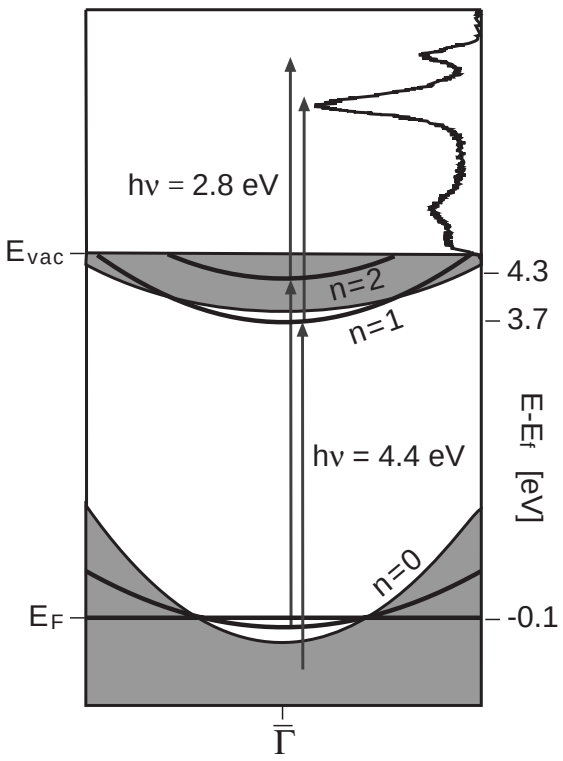

Figure 4.19: Surface projected bulk band structure and dispersion of the n=0-surface state, n=1 and n=2 image potential state together with the TR-2PPE scheme for the Ag(111) surface. Effective electron masses and binding energies taken from [139] and [140] respectively.

and t_0 were determined from measurements on the gold sample. Values of the lifetime and the dephasing time were obtained by fitting the measured curves to the solution of Eq. 2.4.7. This results in values for the lifetime of 25±2 fs and 18±2 fs for the n=1 and n=2 IS, respectively. As can be seen in Fig. 4.19 the n=2 IS is in resonance with the bulk bands. This is the reason why its lifetime was shorter than that of the n=1 state although the wave function of the n=2 state is located further away from the surface. The measured lifetimes are in excellent agreement with the values reported earlier by other groups [115, 116]. The dephasing time had to be fixed at T_2=2T_1 to reproduce t_0, indicating that pure dephasing is much slower than the population decay. However, even a simple rate model reproduces both lifetimes within the error limits as long as t_0 is kept as a free parameter in the model.

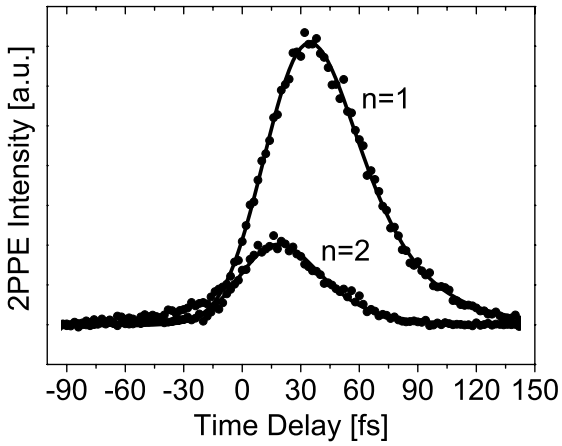

Figure 4.20: Transients for the n=1 and n=2 image potential state at Ag(111) together with the fitted curves obtained from the Bloch model.

4.2.1.3 Ag(110)

The (110) surface of silver does not exhibit a bandgap at Γ in the projected bulk band structure [141]. Accordingly, no IPS are expected. Therefore, and because of the low lying d-bands with respect to Cu and Au, this surface was chosen as the substrate for the adsorbate system Pe'-thiol:Ag(110). For reasons of comparison the bare surface was investigated prior to the adsorbate covered surface.
The experimental setup was identical to that for the measurements on the Ag(111) surface. The background subtracted time resolved energy spectrum (Fig. 4.21) shows a weak 2PPE signal between 1 eV and 2 eV. Two peaks at 2.3 eV and 2.7 eV are observed. The peak at 2.7 eV resembles the width and shape of the crosscorrelation previously measured on the polycrystalline gold sample. The energetic position is consistent with excitation from the Fermi level. The sum of the photon energies (7.25 eV) minus the work function (4.35 eV) gives the kinetic energy of the fastest electrons. The peak at 2.3 eV has a lifetime of around 18 fs and is pumped with the 4.4 eV pulse. The bulk band structure of Ag [142] gives no evidence for the origin of this feature. Ho et al. have predicted a surface band in the bandgap of Ag(110) centered at X [143]. This surface state was measured later by Reihl et al. [141] with AR-IPES. The bandgap does not extend to the Γ point but interpolating the measured and calculated surface state around X to Γ one finds an intermediate state at around 3.8 eV. At Γ the surface state is in resonance with the bulk bands. The binding energy agrees well with the measured peak at 2.3 eV kinetic energy, resulting in 3.85 eV binding energy when the 2.8 eV pulse is the probe pulse and the work function ist 4.35 eV. The lifetime of 18 fs appears to be reasonable when compared to the lifetime of the

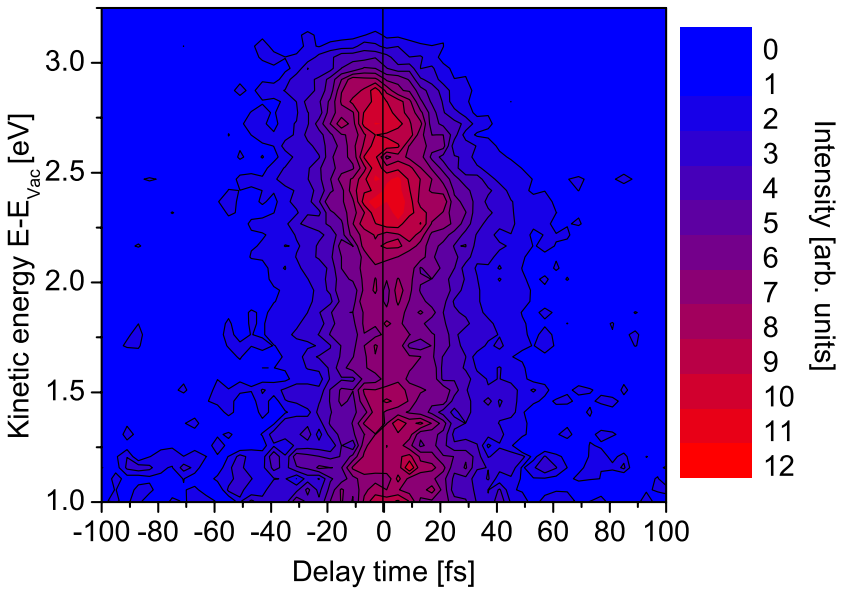

Figure 4.21: 2PPE map of Ag(110) measured with 280 nm + 440 nm pulses.

n=2 IPS of the Ag(111) surface, also being in resonance with bulk states. However, for a reliable assignment further measurements, i.e. polarization dependent and angle resolved 2PPE, are necessary. Fig. 4.21 shows that due to the absence of pronounced peaks and a life-time of sub-20 fs over the whole energy range this surface is suitable as a substrate for adsorbate systems.

4.2.2 TR-2PPE on the bare TiO_2(110) surface

Even though TiO_2 is perhaps the most frequently investigated metal-oxide semiconductor, time resolved 2PPE measurements of a well characterized surface have not yet been reported. Onda et al. have carried out 2PPE measurements on this surface but with the focus on defects and water adsorption. The published 2PPE spectra of the bare surface do not show any significant peaks and have been discussed in terms of changes in the work function [85]. In this work TR-2PPE spectroscopy was carried out with different polarizations, and different photon energies on differently prepared bare TiO_2(110) surfaces.

Figs. 4.22(a) and (b) show TR-2PPE maps of the bare TiO_2(110) surface measured with 4.4 eV and 2.8 eV photon energies where both pulses were p-polarized. The CC of the pulses was 35 fs. The work function of sample (a) was 4.7 eV and a bias potential of 0.5 eV was applied between sample and TOF. It should be noted that the sample was nearly transparent for the 2.8 eV pulse and thus the photoemission yield in this experiment was significantly lower than

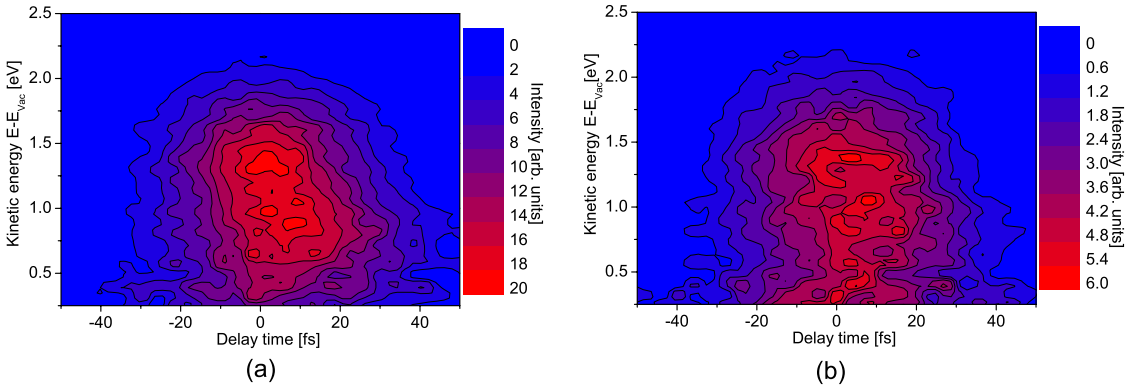

Figure 4.22: Background subtracted 2PPE map of TiO_2(110) with 280 nm + 440 nm, p-polarized. (a) of the vacuum annealed surface, (b) of a surface annealed in O_2 atmosphere (10^{-6} mbar).

at metal surfaces or even adsorbate covered TiO_2. Therefore, the photon fluence of the 2.8 eV pulse was chosen rather high (30 μJcm^{-2}) here but a 3 times smaller fluence gave the same results (compare below). The 4.4 eV pulse was kept as usual at 1 μJcm^{-2}. Under these conditions less than 20 % of the signal was time dependent 2PPE and a large stationary background was subtracted from all the measured signals shown in this chapter. The excited carrier density is estimated to be on the order of 8*10^{17} cm^3 for excitation with the 4.4 eV pulse and 2*10^{14} cm^3 for excitation of occupied gap states with the 2.8 eV pulse.
In addition measurements were done with a reduced fluence of 10 μJcm^{-2} and 0.5 μJcm^{-2} for the 440 nm and 280 nm pulse, respectively, and gave the same results (not shown). Fig. 4.22(a) corresponds to a vacuum annealed surface that was prepared following the standard procedure described in Sec. 3.4.2. Fig. 4.22(b) corresponds to a sample annealed in O_2 atmosphere with a partial pressure of 10^{-6} mbar at 875 K for 10 min. The oxygen pressure was kept constant while the sample was cooled down to 675 K. Further cooling to room temperature was performed under UHV conditions. This sample had a work function of 4.8 eV but no further differences between both samples were noticed in the measurements. The poorer signal to noise ratio in Fig. 4.22(b) was due to a reduced number of scans taken for this sample [3]. Fig. 4.22 shows that the TR-2PPE signal is unaffected by the different preparation procedures.
Although, the signal has completely decayed within 50 fs a temporal shift of the peak signal is observed in Fig. 4.22 between 1.5 and 0.5 eV. To clarify the nature of this feature a measurement identical to that shown in Fig. 4.22(a) was done with the 440 nm pulse s-polarized (Fig. 4.23). Obviously, there is a strong

[3]Fig. 4.22(a) is the sum of 100 scans lasting around two hours.

polarization dependence below 1.1 eV kinetic energy (line in plot). The peak below 0.5 eV (C) in Fig. 4.23 is not polarization dependent and also present in Fig. 4.22(a) but covered by the polarization dependent photoemission (B).

Taking the Fresnel equations, the transmittance of 400 nm light is greater by

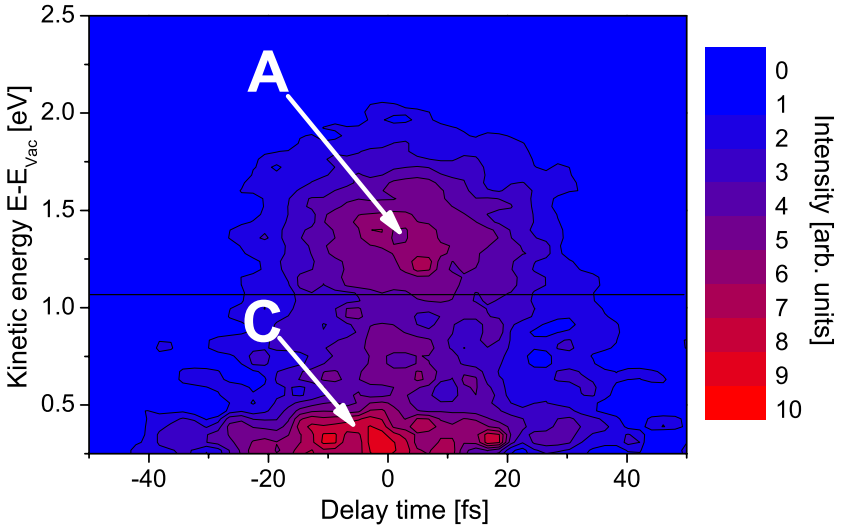

Figure 4.23: Background subtracted 2PPE map of TiO_2(110) with 280 nm p-polarized and 440 nm s-polarized.

a factor of 1.4 for p-polarized light than for s-polarized light at an angle of incidence of 45 °. Fig. 4.24 shows the difference of Fig. 4.22(a) and Fig. 4.23 where the latter values are multiplied by a factor of 1.4. The factor obtained from the Fresnel equations appears to be reasonable since the peak below 0.5 eV does not appear in the difference spectrum anymore. The peak above 1.1 eV (A) is still present but with a reduced amplitude and is thus not completely polarization independent.

From the directions of the temporal evolution of peaks B and C one can deduce the pulse ordering and thus the binding energy of the pertinent intermediate states can be determined. Peak B is pumped with the 4.4 eV pulse and probed with 2.8 eV and has an intermediate state energy of 2.9 eV. For peak C the pulse ordering is inverted and with 4.4 eV probe pulse energy an intermediate state energy of 0.7 eV with respect to the Fermi level is determined. It should be noted that one can not unambiguously deduce the intermediate state energy from the measured kinetic energy for peak A because the pump-probe order is not clear when both pulses overlap.

However, to elucidate the hot electron dynamics in TiO_2 further, monochromatic TR-2PPE measurements were carried out with a different vacuum annealed

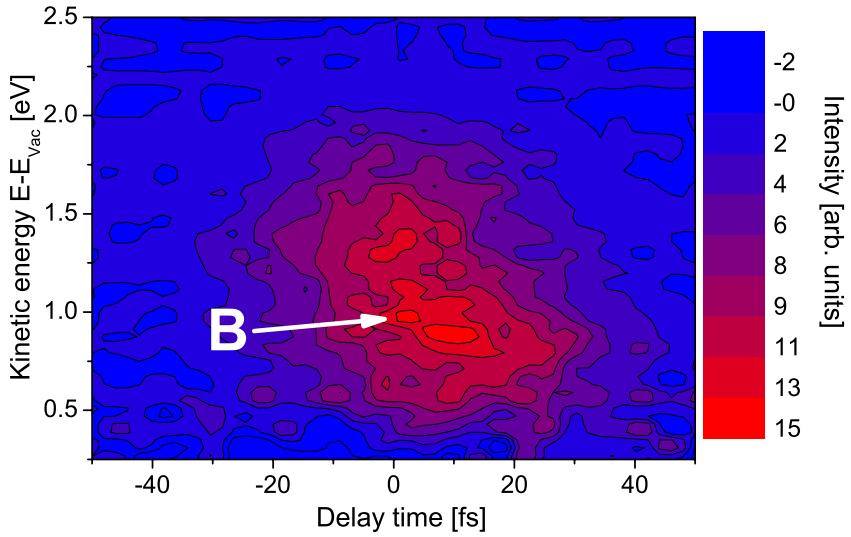

Figure 4.24: Difference spectrum of the p-polarized measurement shown in Fig. 4.22(a) and the s-polarized measurement shown in Fig. 4.23.

sample exhibiting a work function of 4.4 eV. Since the spectra are dominated by 1PPE when both pulse energies are comparable to the work function the photon energy was reduced to 4 eV for these measurements such that the lowest intermediate state energy could be measured at 450 meV. In addition at this wavelength much shorter pulses can be generated resulting in a crosscorrelation of 28 fs for this experiment. The photon fluence was (4.2 μJcm^{-2}) for both pulses and the excited carrier density was estimated to be 2*10^{18} cm^3. Fig. 4.25 shows the 2PPE map measured on the bare (110) surface of TiO_2 rutile with monochromatic p-polarized pulses. The CC was measured prior to the experiment on a Cu(111) sample and afterwards on a polycrystalline gold sample yielding 28 fs and 30 fs Gauss FWHM, respectively. Fig. 4.26 shows the temporal width (FWHM) of a Gaussian fit to time traces extracted at the respective kinetic energies given at the abscissa. The assignment of the kinetic energy to the intermediate state energy is unambiguous here because just one photon energy is used. Above 3.0 eV intermediate state energy the time traces have a width of around 30 fs. Between 3.0 and 2.5 eV the lifetime of the intermediate state is changing and the maximum width of the crosscorrelation of around 40 fs is reached at 2.5 eV intermediate state energy. With this measurement at hand the intermediate state resulting in peak A can be assigned. Peak A is observed with both polarizations and thus the intermediate state is most likely a bulk state. Assuming the pump photon energy either as 2.8 eV or 4.4 eV is compatible with an intermediate state energy of either 3.3 eV or 1.7 eV, respectively. Fig. 4.25 revealed pulse widths of 30 fs and 40 fs for these energies,

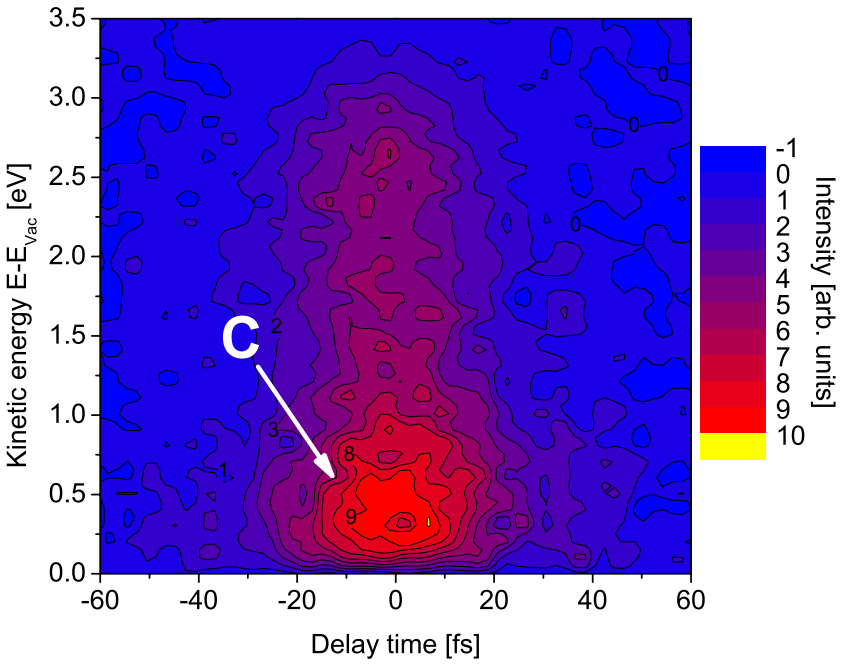

Figure 4.25: Background subtracted 2PPE map of TiO_2(110) with 320 nm, p-polarized.

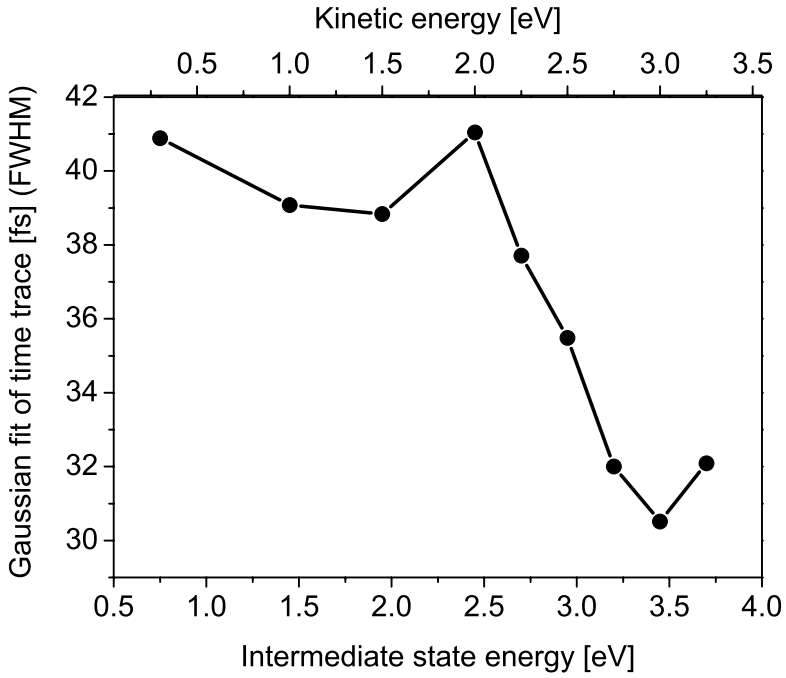

Figure 4.26: Temporal width (FWHM) of a Gaussian fit to time traces extracted at the respective kinetic energies given at the abscissa.

respectively. Since the time trace of peak A gives a width of 35 fs and because the CC for this measurement was also 35 fs the intermediate state energy of 3.3 eV is assumed to be valid.
Peak B is only observed with p-polarized probe light and hence a surface state with transition dipole moment perpendicular to the surface is a possible intermediate state. The lifetime of around 15 fs at an intermediate state energy of 2.9 eV supports this assignment. To ascertain this assumption a TiO_2 sample was sputtered with Ar^+ at 1 kV for 10 min without subsequent annealing. The work function decreased to 4.3 eV. This treatment is believed to destroy the surface order and hence surface states. Fig. 4.27 shows the background

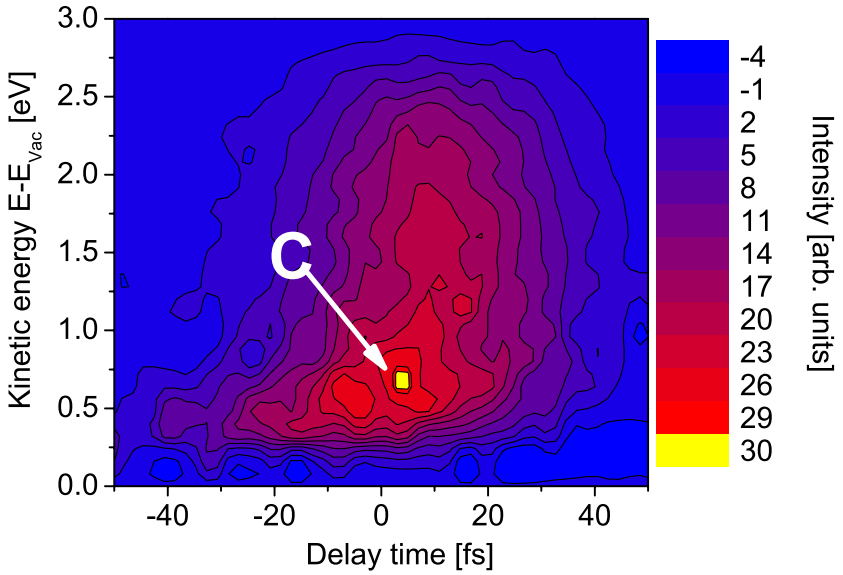

Figure 4.27: Background subtracted 2PPE map of TiO_2(110) with 280 nm and 440 nm p-polarized. Heavily sputtered surface.

subtracted 2PPE map of the sputtered sample. The experimental parameters were identical to those of the measurements shown in Fig. 4.22 and Fig. 4.23 except for the sample bias kept at 0 V because of the reduced work function. The temporal evolution indicates clearly that the signal below 1 eV kinetic energy originates from the same intermediate state energy as peak C. Above 1 eV no prominent feature is observed. This supports the assignment of peak B to a surface state.
The assignment of the different 2PPE peaks to intermediate states together with a plot of the bulk DOS of TiO_2 taken from Ref. [78] is combined in Fig. 4.28. Peak C is assigned to photoemission from unoccupied bulk states. The energetic position roughly corresponds to the increased bulk DOS 1 eV

above the conduction band edge. See et al. have reported inverse photoemission measurements on the nearly perfect and on the defective TiO_2(110) surface [144, 93]. In both measurements they observed a peak slightly below 1 eV energy above the conduction band. A reliable assignment to either bulk or surface state was not possible in this experiments. Nevertheless, they assigned the peak to a surface resonance predicted by Munnix et al. from tight-binding calculations [78]. However, the predicted surface resonance have been reported to be located 0.5 eV above the conduction band edge and thus, 0.4 eV below the peak that has been reported by See et al.. The measured position of peak C agrees well with the reported IPES measurements but the assignment to a surface state is in conflict with the measurements discussed in this section. From the lack of sensitivity to different surface treatments peak C is assigned to photoemission from bulk intermediate states.

In the same publication See et al. have reported a surface state located 2.2 eV above the conduction band edge in agreement with a predicted surface state located 2.5 eV above the conduction band edge. This agrees well with peak B located 2.9 eV above the conduction band that exhibited a pronounced polarization dependence in the photoemission step. Hence, peak B is assigned to photoemission from a surface state.

Peak A is not observed in the IPES measurements that have been reported by See et al. but may correspond to a small shoulder present in the published data around 3.5 eV. It is assigned to photoemission from unoccupied bulk states because of the very short lifetime which is in agreement with the lifetime measured at the same intermediate state energy with a different photon energy.

An assignment of the different transient signals on the bare rutile (110) surface appears to be possible. Nevertheless, the very fast relaxation and decay dynamics have to be discussed. The extremely fast disappearance of the transient 2PPE signals at energies near the conduction band (Peak C) [4] is noteworthy. For example, measurements on reconstructed InP carried out in our group revealed lifetimes of several picoseconds for thermalized bulk electrons at 200 meV above the conduction band minimum [42]. Similar values have been reported for Si [145, 146] and GaAs [147]. Lifetimes comparably short as the ones reported here are known for transition metals where they are ascribed to the large phase space available for electron-electron scattering due to the Fermi level located near the d-bands [29]. The latter argument is certainly not valid for TiO_2 and the very short electron lifetime can hardly be attributed to energy relaxation.

[4] In Fig. 4.27 a kinetic energy of 250 meV corresponds to 150 meV energy above the conduction band edge.

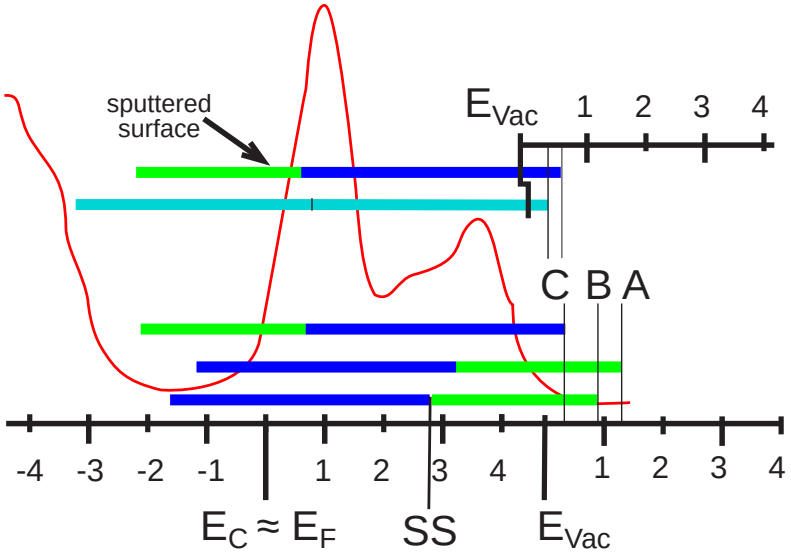

Figure 4.28: Assignment of the different 2PPE peaks to intermediate state energies. 2.8 eV pulse (green), 4 eV pulse (cyan), 4.4 eV pulse (blue). Bulk DOS of rutile TiO_2 (red) [78].

Another mechanism would be the escape of electrons out of the detectable surface region given either by the attenuation length of the light or the escape depth of the electrons. The absorption depth of 440 nm light in TiO_2 is 2 mm estimated from the absorbance of the sample, the escape depth for the excited electrons is not exactly known. The "universal curve" for the inelastic mean free path does not reflect the escape depth for electrons with a very low kinetic energy since elastic scattering has to be taken into account [148]. However, the upper limit according to the "universal curve" is 90 nm at 1 eV kinetic energy [149]. The actual value will be much smaller. For example, calculations on SiO_2 where elastic scattering has been taken into account, have predicted an escape depth of 10-15 Å for kinetic energies between 1 eV and 10 eV [148]. Comparable values have been predicted for GaAs [150]. The escape depth for electrons is orders of magnitude smaller than the absorption depth of the pump light and escape out of the detection range can only occur when there is a net electron momentum away from the surface. In terms of diffusion, certainly not valid in the actual time range, there is no density gradient driving the diffusion. In principle, a dipole moment at the surface could be another driving force for the escape mechanism. Surface dipoles are known e.g. for reconstructed III-V semiconductor surfaces and originate from band bending due to surface states. However, surface dipoles are sensitive to the actual condition of the surface and the measured electron lifetime should depend on the surface treatment, but no differences were observed between the oxygen annealed, the vacuum annealed

and the heavily sputtered surface. Hence, it is unlikely that electron escape is the dominating effect responsible for the short electron lifetime observed even at low intermediate state energies.

Peak C undergoes a shift in energy of around 200 meV in 30 fs before it disappears. This would be compatible with phonon induced intra-band relaxation. The dominant LO phonon modes in rutile TiO_2 have a frequency of 24 THz (100 meV) or a period of 41 fs [151]. Taking the flat conduction bands of bulk rutile (Fig. 2.17) and the narrow angular acceptance of the TOF spectrometer of 0.026 Å into account, it appears unlikely that the shift in energy is controlled by LO-phonon scattering. Another phonon triggered process that results in the loss of signal in TR-2PPE is inter-valley scattering. Scattering times of sub-60 fs have been reported for Γ-L scattering in InP [124]. This process is only possible for electrons with an excess energy higher than the barrier between the Γ and the side valley and can not account for the short lifetimes at low intermediate state energies.

As in most transition metal oxides, the strong electron-phonon interaction caused by the ionic nature of the crystal in TiO_2 leads to the formation of polarons. Polarons with a binding energy of around 400 meV have been reported in Ref. [152]. The 24 THz LO-phonon mode is expected to play an important role in the formation of these polarons [153]. Thus, the observed energy shift can in principle be assigned to the formation of a polaron on the time scale of the dominant lattice vibration. However, a final assertion of the electron dynamics at the bare rutile surface would require further investigations, i.e. dispersion measurements at different time delays (cf. Ref. [154]), and is beyond the scope of this work.

To conclude, the TR-2PPE signal of the bare rutile surface is weak compared to all other systems investigated in this work and decays exceptionally fast.

To ensure that the preparation procedure discussed in Sec. 3.4.2.1 did not lead to any additional background signal in 2PPE for some samples two identical rutile crystals were mounted on the same sample holder with the [001] axis oriented in the same direction. Both samples were prepared identically up to the coating procedure. Only the lower sample was dipped in the solution containing the chromophore. Afterwards, both samples were rinsed with clean solvent to ensure that even the uncoated sample was exposed to the solvent. TR-2PPE measurements on both samples were done by just shifting the sample in front of the TOF. All other parameters of the measurement were kept constant. Fig. 4.29 shows two time traces extracted at the same energetic position (1 eV kinetic energy) and with the same width (200 meV) from the coated sample (black) and

from the uncoated sample (red). The stationary background was subtracted. The small signal from the uncoated sample peaks at t_0. It may have the same

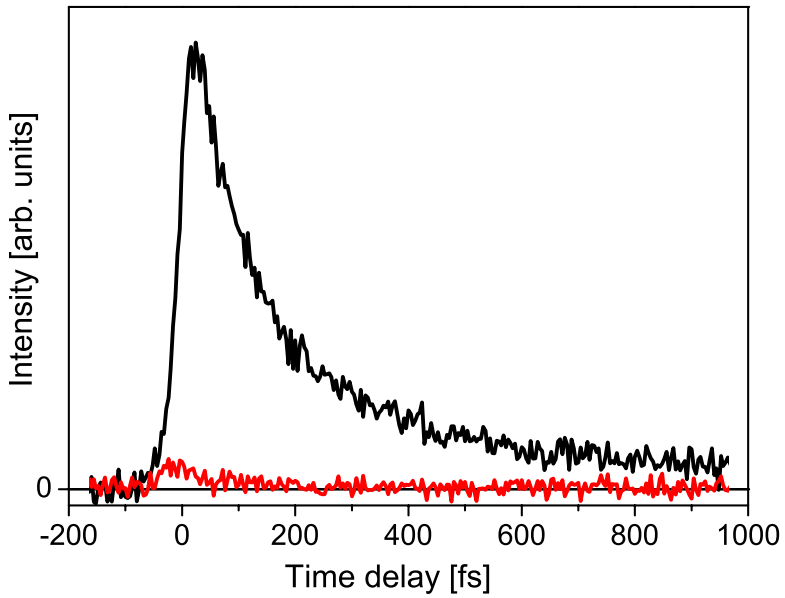

Figure 4.29: Comparison between a TR-2PPE measurement on a sample coated with a chromophore (black) and an uncoated sample (red). Apart from that both samples were treated identical. As an example a measurement on a Pe'-$PO(OH)_2$ coated sample is shown.

origin as the signal discussed above for the annealed TiO_2 surface but it should be noted that a minimal contamination stemming from the solvent can not be excluded. Thus, no further efforts were made concerning this signal. However, for interpreting photoemission from the coated samples this small, short-lived background can surely be neglected. Furthermore, this measurement sheds light on the origin of the small pedestal in the rising edge of all time traces from samples coated with chromophores.

4.3 Time-dependent 2PPE signals in the presence of organic chromophores

4.3.1 Time-dependent 2PPE signals of perylene chromophores attached to TiO_2 via long rigid spacer cum anchor groups

As discussed in Sec. 2.1 the present system is suitable to measure the distance dependence of ET because in the wide band limit the FC term of Eq. 2.1.2 is summed up to yield the factor 1 and the distance dependent electronic coupling is the only remaining term. To do so, different spacer groups were inserted between the chromophore and the anchor group ranging from just one methylene group to rigid spacers with a length of up to 13 Å. The latter molecules showed a pronounced multi-exponential injection time when measured with transient absorption spectroscopy. The first aim of the TR-2PPE measurements on the single crystal surfaces was to clarify whether the different injection times are intrinsic to the molecule or whether they were due to inhomogeneities in the colloidal films. The Pe'-tripod was adsorbed onto two different colloidal films. On an anatase film deposited on 50 μm thick glass and on a rutile colloidal film deposited on 500 μm thick cover-glass. The preparation procedure is discussed in Sec. 3.4.2.1. Fig. 4.30 shows the transient absorption signal of the Pe'-tripod cation. Both

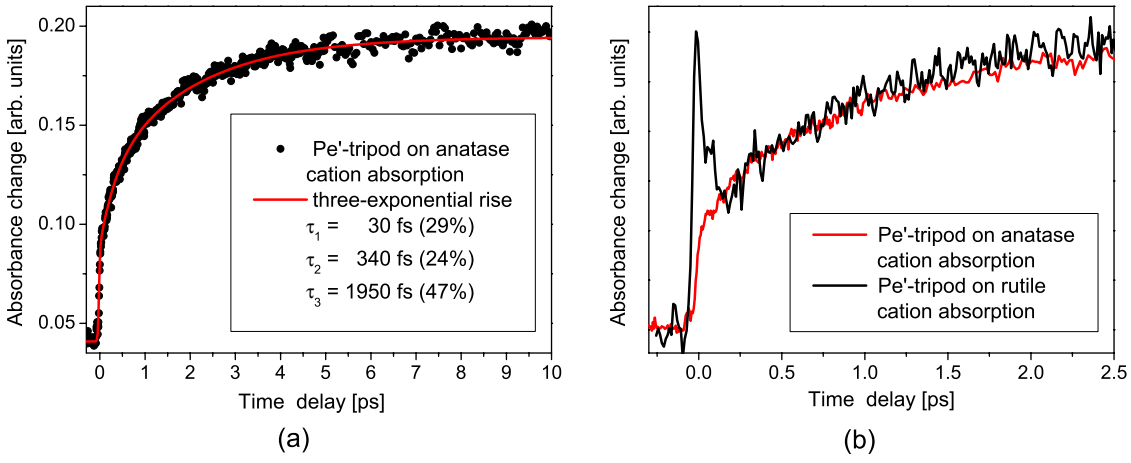

Figure 4.30: (a) Transient absorption signal of the Pe'-tripod cation adsorbed on anatase colloidal film taken from Ref. [64] (black) and three-exponential fit of the signal rise (red). (b) Comparison between cation transient absorption of Pe'-tripod on a rutile colloidal film (black) and on an anatase colloidal film (red).

samples exhibit the same multi-exponential injection dynamics (Fig. 4.30(b)). This assures the validity of comparing transient absorption signals measured on anatase colloidal films with TR-2PPE measurements performed on rutile crystals. The peak near t_0 in the rutile measurement (Fig. 4.30(b) black) is due to non-resonant coherent contributions from the thick glass substrate [155]. The modulations are due to the data acquisition. The transient absorption measurement of the anatase colloidal system was fitted with a rate model representing three different species each injecting on a different time scale. The short time constant of around 30 fs is incompatible with the longer time constants measured in our group on colloidal films for perylene derivatives with much shorter spacer groups. To clarify whether the multi-exponential injection is specific for the colloidal film, TR-2PPE measurements were done with the same molecule on a TiO_2 rutile single crystal.

The preparation is described in Sec. 3.4.2 in detail. The measurement was per-

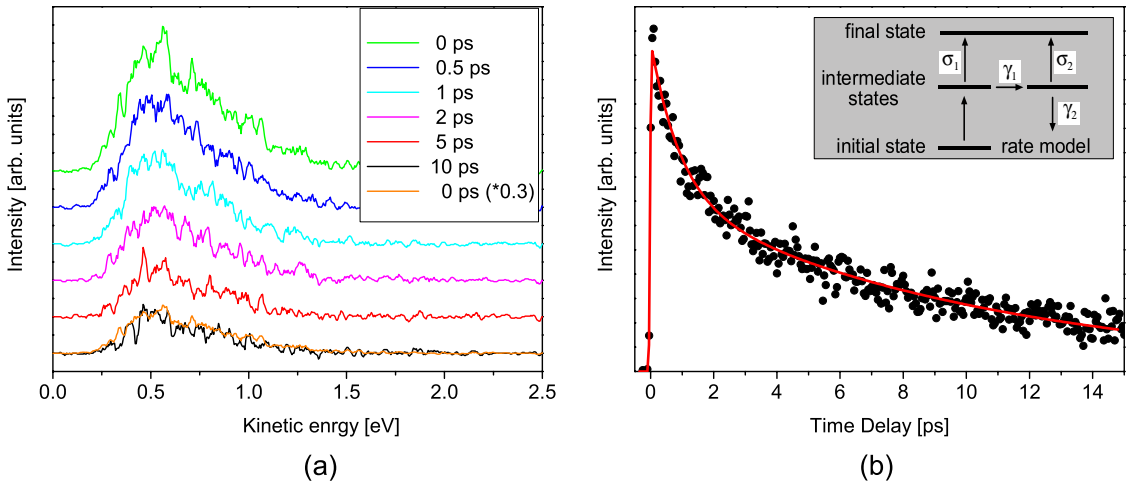

Figure 4.31: 2PPE energy spectra of Pe'-tripod on rutile (110) at different time delays (a). Time trace measured between 350 and 750 meV kinetic energy (dots) and fit with the rate model shown as inset (line) (b).

formed with 440 nm pump pulse (41 μJ cm^{-2}, 17 fs FWHM$_{pulse}$), 285 nm probe pulse (9 μJ cm^{-2}, 45 fs FWHM$_{pulse}$) and a bias voltage of 0 V. Fig. 4.31(a) shows 2PPE energy spectra at different time delays. Energy relaxation is negligible. To illustrate this the time trace at 0 ps is shown a second time (yellow line) scaled by 0.3 on top of the spectrum at 10 ps. As no energy relaxation is observed, a time trace taken at 0.54 eV (Fig. 4.31(b)) reflects the lifetime of the contributing intermediate states. It is obvious that the short time constant observed in the transient absorption measurement is missing. The TR-2PPE measurement was

fitted with a rate model shown in the inset of Fig. 4.31(b) with two rates, but here the second time constant was needed to remove the long-lived background signal ascribed to electrons injected from the chromophore into the conduction band of TiO_2. A detailed discussion of the rate model is given in Sec. 2.4.1. The time constants $\left(\tau_i = \frac{1}{\gamma_i}\right)$ resulting from the fit-model are: $\tau_1 = 1$ ps, $\tau_2 = 12$ ps, with weight factors: $\sigma_1 = 0.95$, $\sigma_2 = 0.05$.
Similar results were obtained by comparing transient absorption measurements with TR-2PPE data for another chromophore with a long rigid spacer group: Pe'-rod. Fig. 4.32(a) shows the transient absorption measurement of Pe'-rod ad-

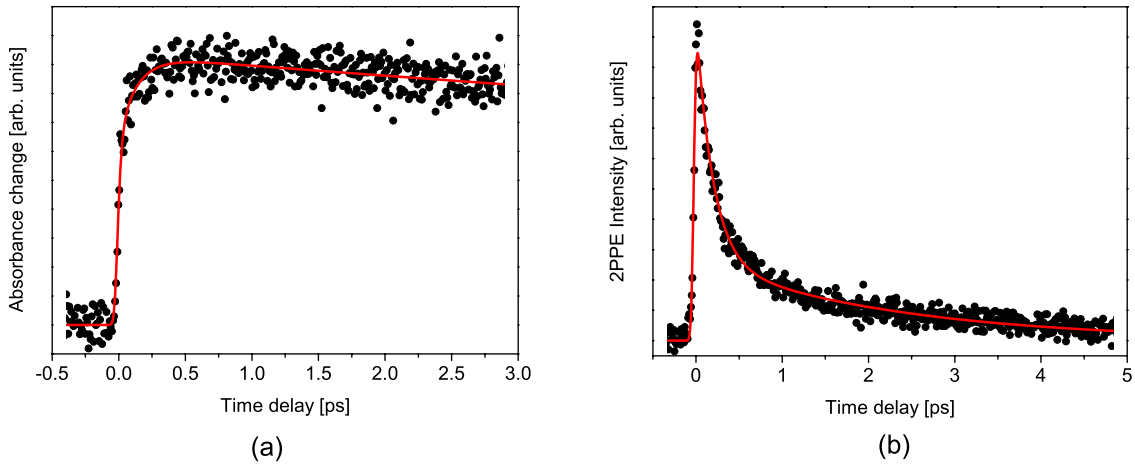

Figure 4.32: Transient absorption signal of the Pe'-rod cation formation when adsorbed on an anatase colloidal film and the fit with a rate model (a). Time trace measured via TR-2PPE in an energy window of 400 meV kinetic energy at the excited state position of Pe'-rod (dots) and fit with the rate model shown as inset in Fig. 4.31(line) (b).

sorbed onto an anatase TiO_2 colloidal film (dots) and a fit with a rate model representing two independent species (line). Fit parameters were:

- injection times $\tau_1 = 30$ fs, $\tau_2 = 235$ fs
- amplitudes $A_1 = 74$ %, $A_2 = 26$ %
- decay times $\tau_1^d = \tau_2^d = 15$ ps.

Again, a short injection time constant is dominating the transient signal. The second time constant of 235 fs is reasonable even though the distance between chromophore and substrate is comparable to Pe'-tripod, because the LUMO orbital of perylene is partially delocalized over the phenyl ring (Fig. 2.10) and

thus, the "effective distance" for ET is smaller, cf. discussion in Ref. [64].
The TR-2PPE measurement of Pe'-rod on a rutile single crystal and a fit with the same rate model used for the TR-2PPE Pe'-tripod measurement is shown in Fig. 4.32(b). The time constants resulting from the fit are: $\tau_1 = 193$ fs, $\tau_2 = 2.3$ ps, with weight factors: $\sigma_1 = 0.96$, $\sigma_2 = 0.04$. As for Pe'-tripod the short time constant measured by TR-2PPE agrees well with the long time constant of the transient absorption measurement, whereas no time constant of the order of some ten fs is observed. The long time constant of TR-2PPE is again of the order of the length oft the time scan.
Both systems show the same properties. The transient absorption signal measured with colloidal films contains a short time constant with a large amplitude which is not expected for an electron donor separated via a long rigid spacer from the acceptor. This short time constant is not present in TR-2PPE measurements on single crystal surfaces. Therefore, it is ascribed to conformational inhomogeneities in the colloidal film, namely to molecules bound in the cavities of the colloidal film such that the chromophore is much closer to an adjacent wall than to the floor where it is fixed with the anchor group. This effect gains importance when the spacer group gets longer. First, for a bigger molecule it is more likely to touch a wall. Both the molecules discussed here are around 25 Å in their long axis and thus only a factor 4 smaller than the mean diameter of the cavities. Secondly, for molecules with shorter spacers the regular time constant for charge transfer in the direction of the bridge becomes comparable or shorter than the time constant for the shortcut to an adjacent wall. Thus, electron transfer in the direction of the anchor group is the fastest process.
Since TR-2PPE turned out as an excellent method to investigate the injection dynamics of dye covered TiO_2 single crystals, measurements were performed with this technique on other perylene derivatives already investigated via transient absorption spectroscopy. It turned out that the TR-2PPE signal for these perylene derivatives with shorter spacer groups or only the anchor groups contained additional contributions that must be ascribed to the injected electrons, as will be shown below.
As an example the transient cation absorption signal for Pe'-COOH adsorbed on TiO_2 anatase colloidal film is shown in Fig. 4.33(a) (dots). A fit with a rate equation gives 13 fs as the rise time for the signal (line). Taking the 13 fs rise time as the injection time of the molecule in the rate equation used to fit the Pe'-rod and Pe'-tripod TR-2PPE data and keeping all other parameters constant results in the red line in Fig. 4.33(b). The black dots are the measured TR-2PPE

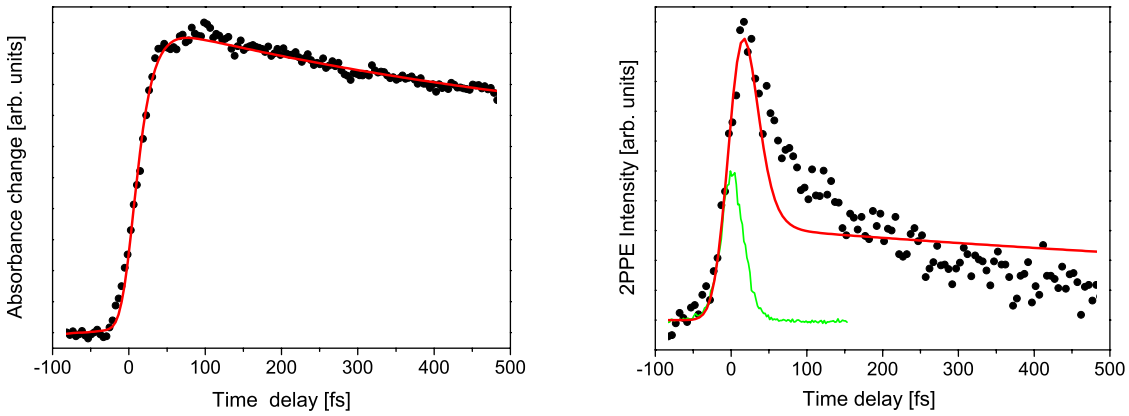

Figure 4.33: Transient absorption signal of the cation formation of Pe'-COOH cation adsorbed on anatase colloidal film and fit with a rate model (a), taken from Ref. [64]. Expected (red line) and measured (black dots) TR-2PPE signal for the same system. CC trace of pump and probe pulse: 34 fs FWHM$_{CC}$.

signal on the Pe'-COOH:rutile system. The CC trace of 34 fs FWHM$_{CC}$ demonstrates the time resolution available in TR-2PPE for measuring molecules with only a short anchor group. Obviously, another process is contributing to the 2PPE signal with a time constant of around 100 fs. The same observation was made with other perylene:rutile systems. Therefore, a detailed investigation was made of the different contributions to the TR-2PPE signal stemming from the perylene derivative and from electrons injected into the TiO_2 substrate. To this end experiments were performed with the perylene chromophores attached to a metal substrate.

4.3.2 Time-dependent 2PPE signals of Pe-thiol chromophores attached to (110) surface of Ag

The perylene chromophore was attached to the (110) surface of a silver single crystal to check whether the additional signal measured in TR-2PPE for perylene anchored with a short spacer group on TiO_2 originates from the molecule or from the substrate. Moreover, such systems are currently in the focus of research because they are model-systems for molecular electronic devices. Chemical anchoring of molecules to noble metal surfaces is commonly performed via a thiolate group. Thiolates are known to form self assembled monolayers (SAM) on the surface of noble metals. In fact these systems are among the most frequently investigated organic adsorbate systems on metals and are candidates for contacting

and/or assembling molecule-based electronic to metals (the molecular "alligator clip" [156, 157]). A review of the electronic structure of metal-organic interfaces with a focus on TR-2PPE is given in [44].
The measurements were performed on perylene-methyl-thiol attached to the (110) surface of silver. It should be noted that in contrast to all other perylene derivatives investigated in this work this chromophore was only available without the bulky tertiary-butyl groups. After cleaning the crystal by cycles of sputtering and annealing, the molecules were adsorbed from solution by using the same procedure as described for the TiO_2 rutile single crystals in Sec. 3.4.

The perylene coated Ag crystal was investigated by means of stationary elec-

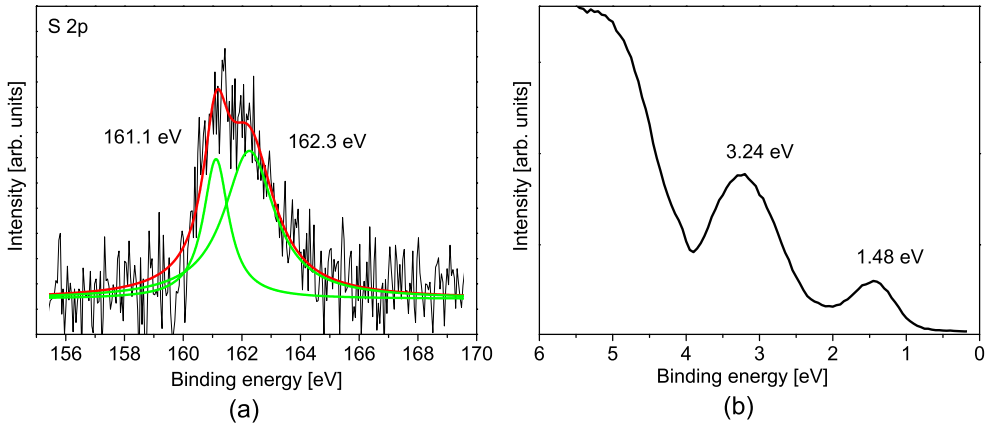

Figure 4.34: (a) XPS S2p doublet emission. (b) HOMO and HOMO-1 of perylene on Ag(110) measured via UPS.

tron spectroscopy. Fig. 4.34(a) shows the XPS S2p doublet emission. The peak position agrees well with XPS measurement of other thiols bound to silver surfaces [158]. The large chemical shift of 2.5 eV is known for sulfur on nobles metals [159] and gives strong evidence for these molecules forming a bond via the thiolate group to silver atoms, as was expected. An UPS spectrum is shown in Fig. 4.34(b). The work function of the sample was 4.1 eV, 200 meV smaller than that of the bare surface. The HOMO and HOMO-1 peaks of the perylene chromophore are clearly visible (cf. Fig. 4.5). The position of the HOMO (1.48 eV, FWHM 700 meV, Gaussian fit) indicates a shift of the IP of 1.5 eV to lower binding energies with respect to the IP of perylene in the gas phase. This effect has also been reported for other aromatic thiolates and was ascribed

for penta-fluoro-thio-phenolate to direct wave function mixing between the adsorbed molecule and the metal surface and to the screening of the hole by the increasing electron density when the molecules form an adsorbate layer [160]. The chromophore investigated here is separated from the sulfur atom by a saturated methyl group. Hence, the mixing between chromophore and substrate orbitals is believed to play a minor role. Thus, the closer distance to neighboring molecules is believed to dominate the stabilization of the hole since the higher polarization energy can screen a localized charge. The higher polarization energy reduces the ionization potential. This effect has been shown for perylene single crystals by Sato et al. [161] where the IP was 5.1 eV and the polarization energy was 1.7 eV. For ∼30 nm thick amorphous perylene films on gold an IP of around 5.5 eV has been reported in Ref. [162] which is in good agreement with our UPS measurements.

In order to estimate the coverage of the surface, the measured XPS data for Ag3d5/2, C1s and S2p were analyzed quantitatively. Using the program "SpecsLab 1.8.2" for a "universal organic compound" relative thicknesses of 1 Å and 14 Å were obtained for sulfur and carbon, respectively. Thio-phenolate is believed to be oriented with a tilt angle of 25° against the surface normal [163]. Assuming a similar conformation on the silver surface for perylene-methyl-thiol, a 14 Å thick overlayer of carbon would correspond to a complete mono-layer coverage. Thus it is likely that the electronic structure as well as the charge transfer dynamics are influenced by intermolecular screening and the formation of 2D bands in the adsorbate layer.

TR-2PPE spectra were measured with a 2.8 eV p-polarized pulse (1.5 μJcm^{-2})

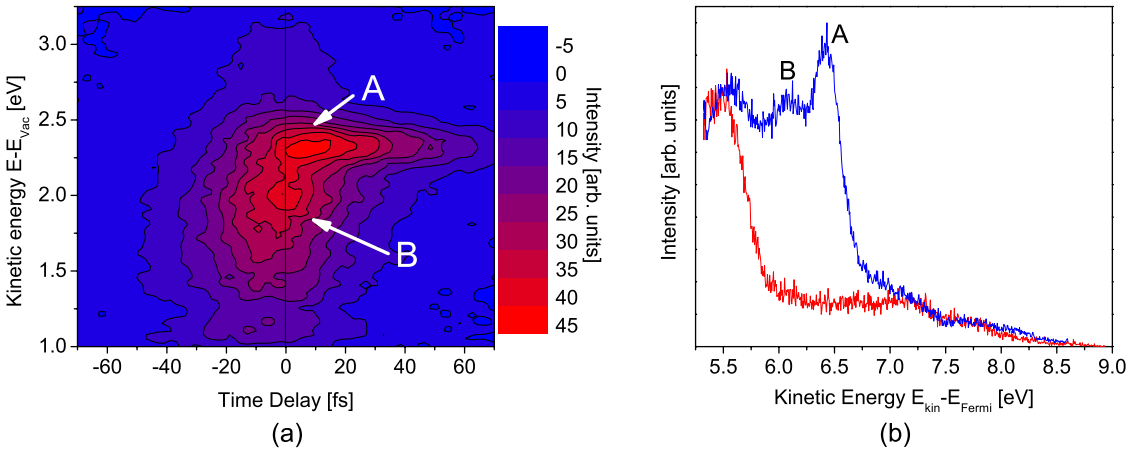

Figure 4.35: Background subtracted 2PPE map of Pe-CH_2-SH adsorbed on Ag(110) with 280 nm and 440 nm p-polarized (a). Comparison of 2PPE from the bare (red) and thiol coated (blue) surface at t_0 (b).

and a 4.4 eV p-polarized pulse (0.5 μJcm^{-2}). In Fig. 4.35(a) a TR-2PPE map is shown measured at -0.5 V bias to suppress the 4.4 eV 1PPE from the Fermi edge. The remaining stationary background from monochromatic 2PPE is subtracted. The time resolved spectrum is characterized by two peaks at 2.0 eV (B) and 2.3 eV (A). Fig. 4.35(b) shows a comparison of 2PPE spectra at t_0 from the bare Ag(110) surface (red) and the Pe-CH_2-SH covered surface (blue). The spectra are normalized to the stationary monochromatic 2PPE emission from the Fermi edge at 5.5 eV. Both peaks clearly originate from the adsorbate layer. Due to the temporal evolution peak (A) can be assigned to a 4.4 eV pump and 2.8 eV probe process and thus, to an intermediate state energy 3.6 eV above E_{Fermi}. Measurements with the 2.8 eV pulse s-polarized showed that emission from peak A was strongly reduced (Fig. 4.36), whereas significant photoemission was observed at energies below peak B. Comparison of the energy spectra taken at t_0

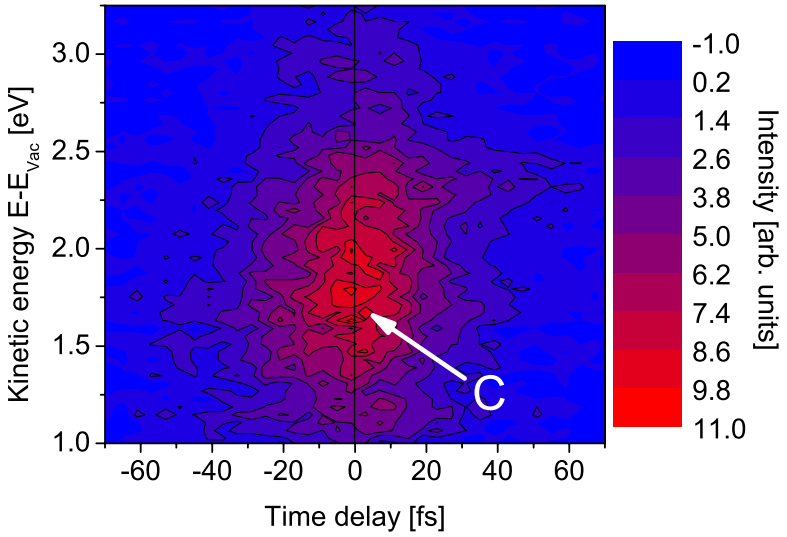

Figure 4.36: Background subtracted 2PPE map of Pe-CH_2-SH adsorbed on Ag(110) with 280 nm p-polarized and 440 nm s-polarized. All other experimental parameter were identical with those in Fig. 4.35

for both polarizations revealed that the peak observed with s-polarized light (C) is located around 300 meV below peak B. In Fig. 4.37 the stationary background was subtracted, apart from that data in Fig. 4.37 (circle) and Fig. 4.35(b)(blue) are identical. The spectra were not normalized and measured under identical conditions. The spectra were fitted with 3 and 4 Gaussians, Fig. 4.37(a) and Fig. 4.37(b), respectively. First, the p-pol spectra were fitted with all parameters free, afterwards the s-pol spectra were fitted with only the amplitudes of the 4(3) peaks as fit-parameters. The peak around 2.8 eV is most likely bichro-

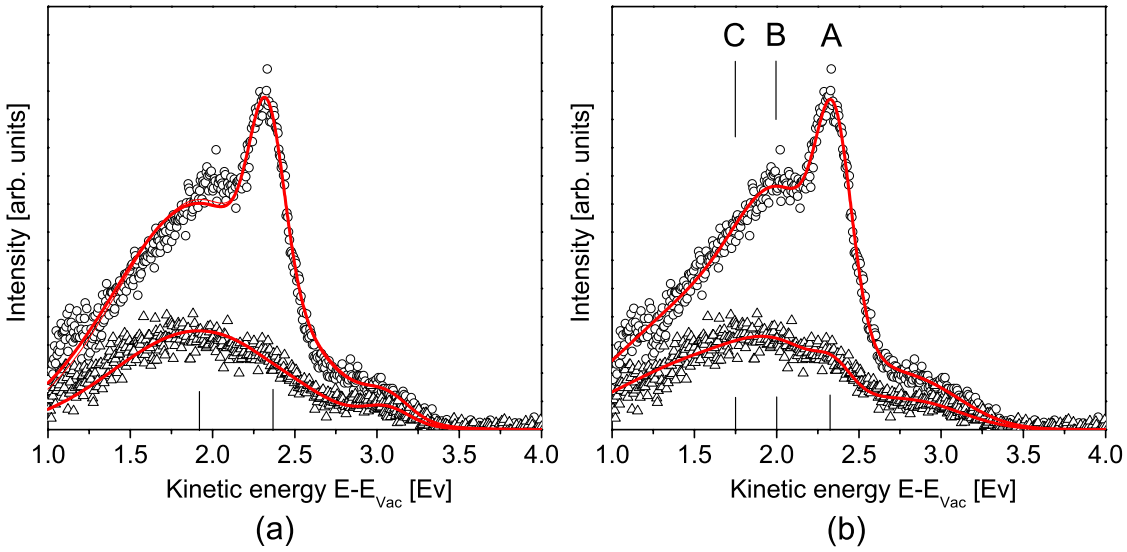

Figure 4.37: Background subtracted 2PPE at t_0 with the 2.8 eV pulse p-polarized (circle) and s-polarized (triangle). The same spectra were fitted with 3 (a) and 4 (b) Gaussians. The peak positions are indicated by vertical lines.

matic photoemission from the Fermi edge of Ag. Obviously, the structure below 2.2 eV can not be fitted well with only one Gaussian function. This is most striking at the 2 eV shoulder. Thus, peak C is also observed in the p-pol spectrum but covered by peak B, and the spectra were fitted with 4 Gaussian functions (Fig. 4.37(b)). The amplitude ratios for p-polarization to s-polarization for the peaks A, B, and C are 10/1, 3.5/1, and 1.8/1, respectively. For the bulk peak at 3 eV again a ratio of 1.8/1 is obtained. The ratio for the absorbance between p-pol and s-pol light in Ag with an angle of incidence of 45° is 1.93 as calculated from Fresnel's equations (n = 0.17, k = 2.4 at hν = 2.8 eV [135]). Thus for peak C and the peak at 3 eV the initial and/or intermediate state is most likely a bulk state. Whereas, the transition dipole moment for peak B is at least partially and for peak C strongly oriented in surface normal direction. The Gaussian fit revealed a line width of 200 meV and 550 meV for peaks A and B, respectively. The assumption that peaks B and C originate from different processes is supported by the temporal evolution of the spectrum at 2 eV kinetic energy. For fitting the time traces extracted from Fig. 4.35 with a rate model, the pulse-width and t_0 were taken from a time trace just below the high energy cutoff of the spectrum (3 eV) in Fig. 4.35 and the width was found identical to a CC recorded prior to this measurement. A time trace taken from Fig. 4.35 at 2 eV kinetic energy and 300 meV width can not be fitted with a mono-exponential rate equation when t_0 and the width are fixed at the values taken from the fit at 3 eV, because the peak positions of both time traces are nearly equal although the

respective width is not. A Gaussian fit of the time traces revealed t_0=0 fs (0.4 fs) and w_{FWHM}=38.9 fs (49.1 fs) at 3 eV (2 eV). Thus the shift of the maximum of peak B against t_0 is too small. This finding is compatible with two intermediate states, one populated with the 2.8 eV pulse (1.6 eV intermediate state energy) the other with the 4.4 eV pulse (3.3 eV intermediate state energy). A fit with two independent rate equations accounting for the proposed dynamics revealed lifetimes of 8 fs and 15 fs for the 3.3 eV and 1.6 eV intermediate state energies, respectively. The time trace at 2 eV kinetic energy (circles), the Gaussian fit of the CC from the same sample at 3 eV kinetic energy (blue), and the fit with the rate equations (red) are shown in Fig. 4.38(a). For comparison, Fig. 4.38(b)

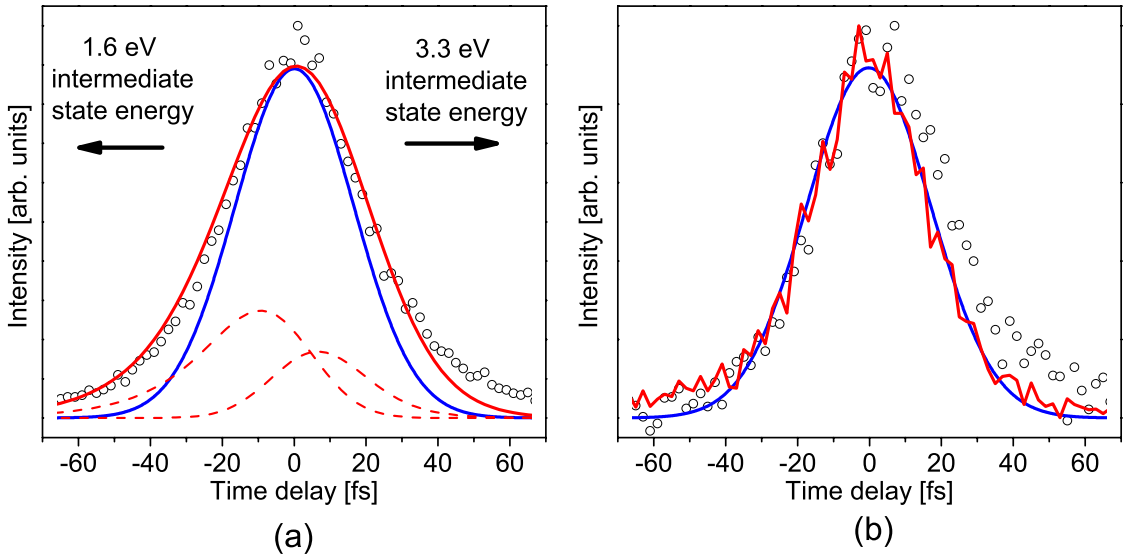

Figure 4.38: (a) The time trace at 2 eV kinetic energy (circles), the Gaussian fit of the CC from the same thiol-coated sample at 3 eV kinetic energy (blue), and the fit with the rate equations (red). The red line is the scaled sum of the two dashed red lines. The arrows indicate the intermediate state energy determined from the pulse ordering. (b) Time traces are shown at 2 eV (circles) and 3 eV (red line) kinetic energy from the clean Ag(110) sample and a Gaussian fit of the latter (blue line).

shows the same measurement on the clean Ag(110) surface. Time traces at 2 eV (circles) and 3 eV (red line) kinetic energy and a Gaussian fit of the latter (blue line) are shown. The time trace at 3 eV (red line) resembles the CC measured on a polycrystalline gold sample. The decay at positive delays (3.3 eV above E_{Fermi}) is observed for both samples and can be assigned to photoemission of hot electrons in the metal substrate. This is supported by the measurement with the s-polarized 2.8 eV pulse where the time trace at 1.75 eV showed the same

temporal dependence as a time trace on the clean sample measured with a p-polarized 2.8 eV pulse. The lifetime of 8 fs for electrons in silver 3 eV above E_{Fermi} agrees well with reported measurements and prediction from Fermi liquid theory [29]. Surprisingly, emission from hot bulk electrons with binding energy of 1.6 eV (negative delay) is not observed. At this energy the lifetime of the electrons has been reported to be longer than 10 fs [29] and should thus lead to a clear deviation from the CC trace at negative delays that is not observed with the clean silver sample (Fig. 4.38(b)). The lifetime of peak A is nicely fitted by a rate model with an instantaneous rise and a mono-exponential decay resulting in a lifetime of 23 fs.

In addition, angle resolved measurements were performed. The energetic positions of peaks A and B were fitted with Gaussian functions and plotted against the parallel momentum in Fig. 4.39. Peak A shows dispersion and can be approximated with a parabola of effective mass $2.8 \cdot m_e$ and energy $E(k_{||}=0)=2.28$ eV. Peak B is nondispersive.

Summarizing, three unoccupied states are observed on the Pe-CH_2-SH covered

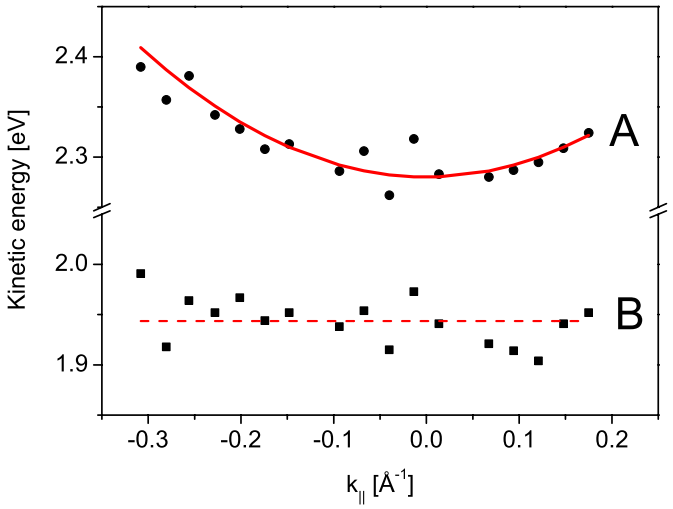

Figure 4.39: Dispersion of peak A (circles) and B (squares). Dispersion for peak A is approximated with a parabola of effective mass $2.8 \cdot m_e$ and energy $E(k_{||}=0)=2.28$ eV (line). The straight dashed line is a guide to the eye.

surface of silver:

- Peak A originates from an intermediate state at 3.6 eV above E_{Fermi} with a FWHM of 200 meV. It is instantaneously populated and has a lifetime of 23 fs. It has a weak positive dispersion with effective mass of $2.8 \cdot m_e$. It is strongly polarization dependent in the photoemission step with dipole

moment nearly normal to the surface.

- Peak B is assigned to photoemission from an intermediate state at 1.6 eV above E_{Fermi} and has a width of 550 meV. It is nondispersive within the resolution capability of the experiment and has polarization dependence in the excitation step. The lifetime of peak B is 15 fs.

- Peak C involves states at 3.1 eV above E_{Fermi} and has a width of 750 meV. Its polarization dependence follows that of the sample absorbance. The temporal evolution of the TR-2PPE signal from the adsorbate covered surface is comparable to that of the clean Ag(110) surface at the same energy. The lifetime is shorter than 10 fs.

The different 2PPE processes leading to the observed peaks discussed above are summarized in Fig. 4.40. In conclusion, peak C is most likely induced

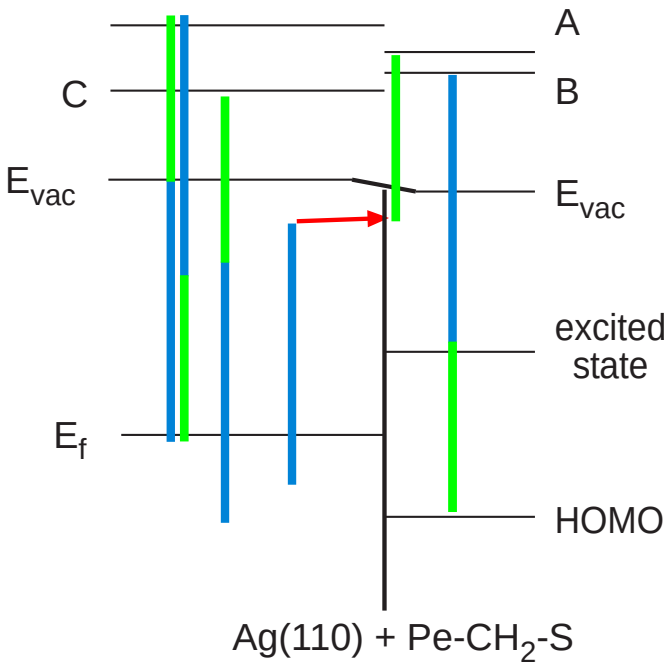

Figure 4.40: The processes leading to the different observed peaks. The green and blue lines represent the 2.8 eV and 4.4 eV pulses, respectively.

by photoemission from hot electrons in the bulk of the substrate. Peak B is clearly adsorbate induced. The energetic position relative to the Fermi level of the substrate agrees with the expected position of the excited state of the perylene chromophore and the polarization dependence is compatible with the chromophore standing upright and tilted by a small angle with respect to the

surface normal direction. The lifetime, e.g. the injection time form the excited chromophore into the metal, of 15 fs appears reasonable compared with other perylene injection systems investigated in this work. Therefore, peak B is attributed to photoemission from the excited state of perylene. Peak A is also adsorbate induced. Because of the width of only 200 meV the orbital of the pertinent intermediate state is not expected to reside on an individual chromophore, otherwise it should exhibit a Franck-Condon broadening comparable to that of the HOMO and the first excited state. Also the long lifetime of 23 fs contradicts the assignment of peak A to photoemission from a higher excited perylene state. Vondrak et al. have reported measurements for different thiolates attached to Cu(111) surface [164]. They observed two molecular resonances independent of the nature of the hydrocarbon group. One is ascribed to photoemission from an intermediate state 3.2 eV above the Fermi level, the other to a final state 6.3 eV above E_{Fermi}. Both states are believed to be localized at the C-S-Cu anchor. Both peaks have a higher photoemission yield for p-polarized light and are reported to have dispersion. Although, the energetic position of the reported final state is in principle compatible with peak A, the measured finite lifetime for peak A is in contradiction to a final state, since a final state is populated via a resonant two photon process and thus its time dependence must be that of the cross-correlation. The energetic position of the reported intermediate state 3.2 eV above E_{Fermi}, the polarization dependence and the dispersion would in principle also agree with peak A provided that small deviations can be ascribed to the different substrates. The comparably long lifetime of peak A and the dispersion are in conflict with a localized orbital.

Lifetime and linewidth of peak A would in principle agree with the emission from an image potential state. Because the (110) surface of Ag has no surface projected band gap and no IPS is observed on the clean sample, the confinement of the image potential on the surface side may be realized in the present case by the molecular layer. Velic et al. have reported measurements on benzene layer covered Cu(111) [165]. They have observed an IPS for a bilayer coverage. Energetic position, effective mass and lifetime are comparable to the values reported here. The high effective mass and the unexpected short lifetime have been explained in terms of a lateral periodic modulation of the image potential caused by the conformation of the benzene molecules on the surface. Other examples for IPS at noble metal surfaces in the presence of dielectric layers are reported in, e.g. Ref. [166, 167].

In principle peak A can be assigned to an IPS. The lateral periodicity can be assigned to the well known “herring bone” structure of the α-phase of perylene

crystals. However, an unambiguous assignment requires further investigations, e.g. measurements on the perylene chromophore substituted with the bulky tert-butyl groups, where a different packing and interaction of the molecules on the surface can be expected.
To conclude, the above measurements showed that the injection time for the excited state of Pe-CH_2-SH on the surface of Ag(111) is around 15 fs and that no long-lived background signal is observed for perylene attached to a metal surface. Thus, the long-lived background described in the previous section for perylene on TiO_2 may be attributed to specific properties of the TiO_2 surface. To investigate this long-lived background further, a special system is discussed in the next section, where no contributions are expected to arise from excited molecular states.

4.3.3 Time-dependent 2PPE signals of catechol adsorbed on TiO_2

To obtain TR-2PPE measurements under the above conditions catechol was adsorbed on the surface of a rutile (110) single crystal. The wet-chemistry preparation of the interface was performed in the specifically designed UHV chamber described in Sec. 3.2.2.
Electrons were photo-generated on the surface of the solid instantaneously by exciting the charge-transfer transition in the catechol:TiO_2 surface complex [168, 169, 170]. The formation of the charge transfer complex on the surface leads to a new broad absorption band centered around 2.8 eV photon energy [170, 169, 171]. Semi-empirical calculations by Persson et al. have confirmed that a direct optical charge transfer lifts the electron from the catechol π-HOMO orbital into empty Ti(3d) states on the TiO_2 surface [172]. In particular, the excited state of catechol is not involved in the processes considered here.
Sub-picosecond mid-IR and visible transient absorption spectra have been reported that showed the electrons arriving in Ti(3d) states within less than 100 fs [170], as was expected for generation in a direct optical transition.
The injection dynamics investigated here are quite different from those where the electron resides first on the excited neutral molecular donor state, e.g. the excited singlet state of a perylene chromophore separated from the TiO_2 surface by a molecular spacer with saturated C-C bonds. In the latter case the electron injection time has been identified with the transfer of the electron from the molecular chromophore into the empty electronic states of the semiconductor [58, 59].

In contrast, when the electron is generated on the surface of the semiconductor simultaneously with the absorption of a photon, as in the present case of the catechol:TiO_2 system, the release of the electron from the surface complex into the bulk remains as the time scale of electron injection [173]. In the general case, however, the escape dynamics measured in the present experimental system are preceded by the transfer of an electron from the molecular donor species into empty electronic states in the surface region of the solid, and the latter process can contribute further time constants.

Transient absorption measurements of the ground-state bleach were carried out, since fast recombination of electrons and holes in the surface charge transfer complex can in principle compete with the escape of the photo-generated electrons from the near surface region into the bulk. Recombination, i.e. repopulation of the ground state, is difficult to measure with TR-2PPE. Therefore, the transient ground-state bleach was measured in ultra-high-vacuum for catechol attached to colloidal anatase TiO_2 films. Extensive investigations of both these systems, i.e. nano-structured anatase films and rutile TiO_2(110) single crystals, in our group have revealed very similar time constants for corresponding electron transfer processes. Thus, the recombination time measured with transient absorption can be taken as an order of magnitude time scale also for the recombination time in the catechol:TiO_2 rutile system.

The position of the catechol HOMO adsorbed on the rutile surface was measured by ultraviolet photoemission spectroscopy (UPS) 1 eV below the Fermi level and thus 2 eV above the valence band edge. Fig. 4.41 shows the photoemission from occupied states gathered from the UPS measurement (dashed line) together with photoemission from unoccupied states taken from the 2PPE measurement (solid line). The UPS spectrum of the bare TiO_2 surface is also shown (dotted line). It was assumed that the high kinetic energy cutoff of the measured energy distributions corresponds to the catechol→catechol$^+$ 0,0 transition of the photoemission process and that the distribution measured at lower energies was controlled by the Franck-Condon factors of the transition. The reorganization energy is very large, about 1.2 eV. A significant distortion is expected upon ionization of a small molecule [5]. The direct optical charge transfer transition from the HOMO of catechol to the empty acceptor states at the surface of TiO_2 instead of electronic states in vacuum should be governed by the same Franck-Condon factors. Excitation of the adsorbed catechol with fixed photon energy generates an ener-

[5]Reorganization energies of similar magnitude can be seen in the optical charge transfer spectra of molecular donor-acceptor pairs when the change in the dipole moment due to the charge transfer transition is large.

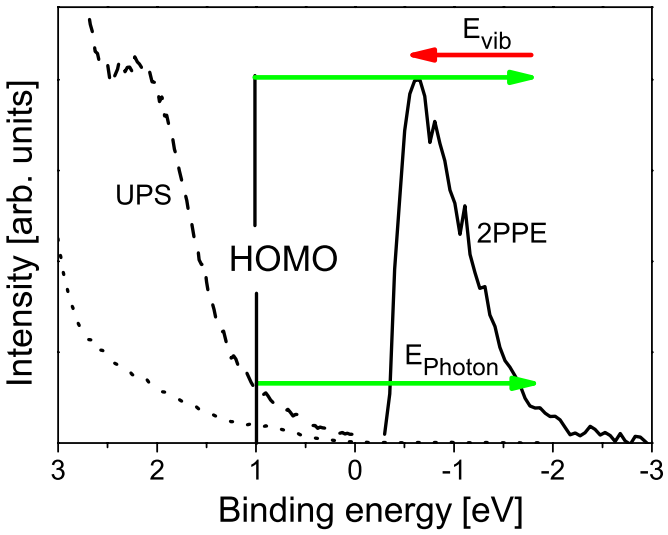

Figure 4.41: The photoemission from occupied states obtained from the UPS measurement (dashed line) together with photoemission from unoccupied states that are populated via the Franck-Condon controlled optical charge transfer transition. The latter spectrum was obtained from the 2PPE measurement (solid line). The UPS spectrum of the bare TiO_2 surface is also shown (dotted line).The HOMO position of the catechol is marked.

getic distribution of the electrons over the empty electronic levels in TiO_2 that is controlled by the magnitude of the respective Franck-Condon factors and by the density of electronic states at the respective energies. The Franck-Condon factor is due to the vibrational excitation of the second product state, i.e. the ionized catechol. The photon energy is partitioned between these two different product states. Thus, in the case of the 0-0 transition the photon energy goes completely into the energy of the respective electronic product state with the highest energy (lower green arrow in the Figure). The corresponding electron population is small since the very small 0,0 Franck-Condon overlap gives rise to only a very weak transition. The population of the electronic states lower down in the conduction band is increasing due to an increasing magnitude of the respective Franck-Condon factors. The partitioning of the photon energy is illustrated in the above Figure for the case of the maximum Franck-Condon factor (photon energy: green arrow, vibrational energy: red arrow).

To test whether the measured VIS-absorption spectrum is consistent with the proposed excitation mechanism a simple model was used. Assuming equal oscillator strength for all transitions the joint density of states resembles the absorption spectrum. The joint density of states (JDOS) between the vibrational density of states (DOS_{vib}) of catechol and the electronic DOS (DOS_{ele}) of unoccupied states

in the conduction band was calculated. DOS_{vib} simulates the Franck-Condon factors for the catechol to ionized catechol transition. The latter was taken from the UPS measurement. DOS_{ele} was taken from a tight binding calculation [78].

$$JDOS(E_P) = \sum_{E=0}^{E_P} DOS_{vib}(E_F - E_P + E)\, DOS_{ele}(E_F + E) \tag{4.3.1}$$

E_P represents the photon energy. In Fig. 4.42 the calculated JDOS (line) and the measured absorption of catechol on a rutile colloidal film is shown. The width of the JDOS is roughly in accordance with the absorption spectrum.

Semi-empirical calculations of catechol adsorbed on anatase TiO_2 have shown

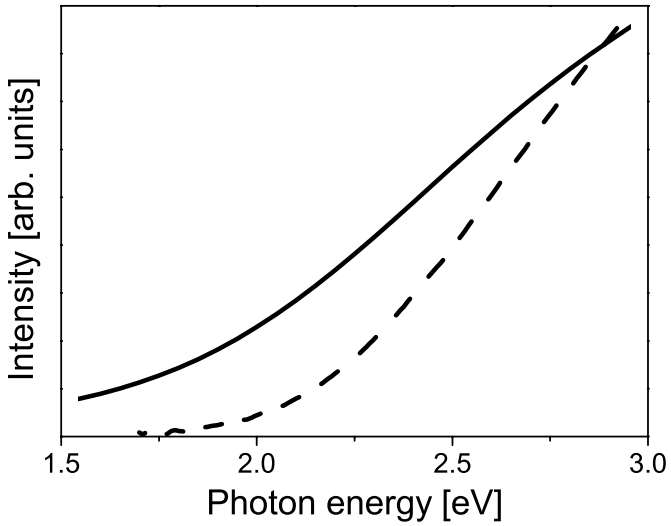

Figure 4.42: Calculated JDOS and measured absorption spectrum of catechol on rutile colloids.

that the HOMO of catechol should be located in the band gap of TiO_2 near the valence band edge [172]. In the latter work the optical transition has been assigned to electrons lifted from the electronic ground state of catechol to Ti(3d) states near the bottom of the conduction band. The calculation has considered only electronic states and has neglected vibrations in the catechol:TiO_2 complex which is an obvious oversimplification of the actual experimental system.

The absorption depth of 300 nm light in TiO_2 is 90 nm [135], the escape depth for the excited electrons is not exactly known. The "universal curve" for the inelastic mean free path does not reflect the escape depth for electrons with a very low kinetic energy since elastic scattering has to be taken into account [148]. However, the upper limit according to the "universal curve" is 90 nm

at 1 eV kinetic energy [149]. The actual value will be smaller. For example, calculations on SiO_2 where elastic scattering has been taken into account, have predicted an escape depth of 10-15 Å for kinetic energies between 1 and 10 eV [148]. Comparable values have been predicted for GaAs [150].

Transient absorption was measured with 440 nm pump and 480 nm probe pulses. Wang et al. have carried out transient absorption spectroscopy on a similar system in solution [174]. They have found that the transient spectra of catechol on TiO_2 colloids do not show any significant spectral shift. An isosbestic point at 510 nm separates the ground state bleach ranging from 420 to 510 nm from the transient absorption of the injected electrons. The reported bleach recovery kinetics are multi-exponential with 62 % of a 0.4 ps component, 19 % of a 8 ps component and longer components. Fig. 4.43 shows the bleach recovery kinetics measured by transient absorption spectroscopy in UHV together with a biexponential fit. Most of the signal recovered within >10 ps. The fast recombination rate of 0.5 ps can be attributed to electrons trapped in shallow traps in the vicinity of the molecules. Whereas the time constants measured here are comparable to the reported ones, the amplitude ratios are not. This difference may be due to the different environments or to a slightly different preparation of the colloids. Nevertheless, the transient absorption signals show that the early depopulation kinetics of the excited state as measured with TR-2PPE are not dominated by recombination but controlled by the escape of the generated electrons from the surface into the bulk as probed

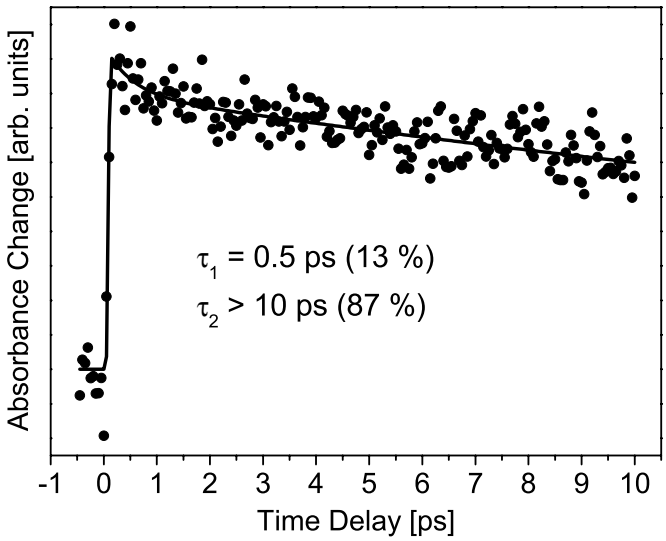

Figure 4.43: Transient bleach of catechol ground state measured at 480 nm after 440 nm excitation (dots). Biexponential fit of the data with the printed parameters.

by 2PPE.

Kinetic energy distributions were measured at different delay times between pump and probe pulse. As the energy of the pump pulse was smaller than the band gap of TiO_2 the bare surface of rutile contributed just a weak 2PPE signal originating from defect induced occupied gap states (cf. Sec. 4.2.2). The corresponding 2PPE background signal was distributed over a wide energy range showing the same time dependence as the CC, thus indicating a very fast decay. The energy of the probe pulse was close to the work function of the sample (4.5 eV). The corresponding one-photon photoemission signal was subtracted from the 2PPE signal. Fig. 4.44 shows 2PPE energy distributions measured at different time delays. The spectrum for zero delay has a maximum at 0.6 eV and a long tail to higher energies. The contributions above 1.8 eV decay very fast and are attributed to the bulk background signal of the sample. A time trace at 2 eV is shown in Fig. 4.45 giving the identical CC of both pulses as found on a Cu(111) single crystal. The exact position of time zero (t_0) and the pulse width were extracted at this kinetic energy. The measured kinetic energy spectrum is assumed to reflect the energy distribution of the electrons injected via the direct optical charge transfer transition due to the photons in the pump pulse. The partitioning of the photon energy between electronic energy in the unoccupied electronic states of TiO_2 and the respective vibrational energy generated in the ionized catechol molecule is illustrated in Fig. 4.41. The probability of the respective transition and thus the corresponding electron population generated in the empty electronic states of TiO_2 is controlled mainly by the

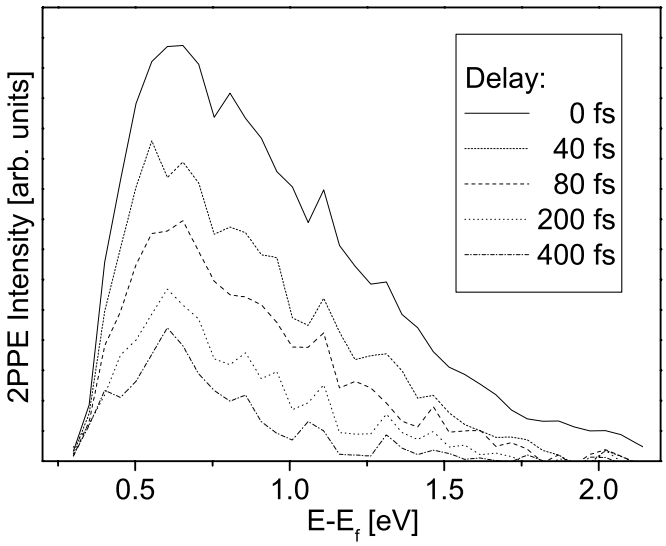

Figure 4.44: Excited state energy spectra for the catechol coated rutile TiO_2 surface at different time delays.

Franck-Condon factors for the transition from catechol to ionized catechol and by the density of unoccupied electronic states in TiO_2. Thus, width and shape of the kinetic energy spectrum with a peak at 0.6 eV is expected to be similar to the ground-state photoionization spectrum measured by UPS and to the linear ground state absorption spectrum of the catechol:TiO_2 charge transfer complex [170, 171]. The peak position is consistent with the measured peak position of the molecular HOMO 2 eV above the valence band edge when the 2.8 eV photon energy of the pump pulse is taken into account (cf. Fig. 4.41). We conclude that the measured kinetic energy spectrum is controlled by Franck-Condon factors for the photoionization of the catechol:Ti charge transfer complex. Fig. 4.44 shows that very surprisingly energy relaxation of the injected electrons is negligible in the present system. For delay times up to 300 fs neither the peak position nor the shape of the spectrum have changed. For comparison energy relaxation is known to occur on a 150 fs time scale in III-V semiconductors [41]. This unusual behavior of TiO_2 is attributed to the electrons residing in states with virtually no dispersion, and there is only very slow energy exchange between these different states. This is supported by band structure calculations revealing a high effective mass for conduction bands at Γ (Fig. 2.15) [3, 78].

Since recombination has been excluded by the above described measurement

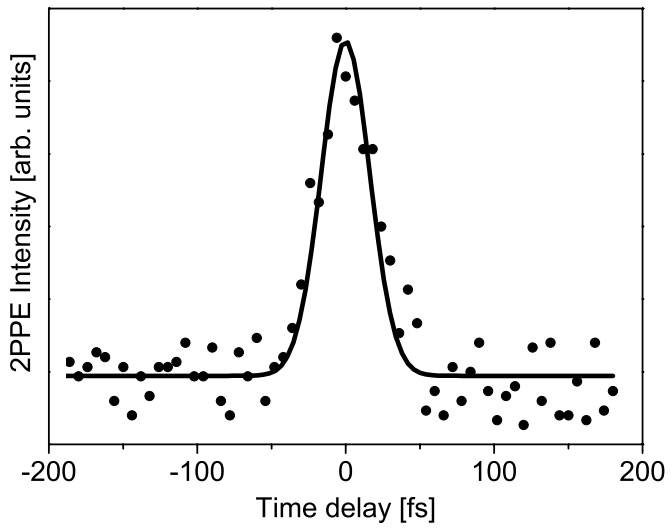

Figure 4.45: Time trace at 2 eV intermediate state energy measured on the catechol coated sample rendering the crosscorrelation of pump and probe pulse (circles) and a Gaussian fit with FWHM of 35 fs (line).

as cause for the long tail of the time dependent 2PPE signal in Fig. 4.46 and since furthermore a very high photocurrent efficiency is known for the dye:TiO_2

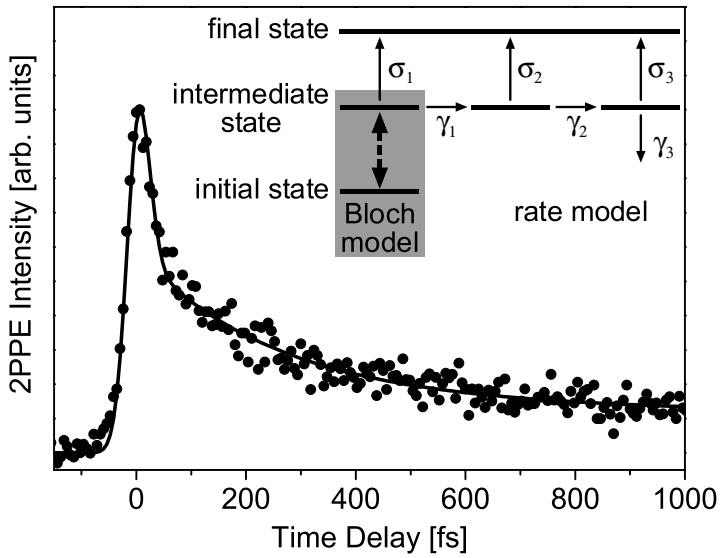

Figure 4.46: Time trace at 600 meV intermediate state energy (circles) and fitted curve using the model shown in the inset (line).

system, the long tail in Fig. 4.46 is attributed to the escape of the injected electrons into the bulk of the rutile crystal. Thus, the escape of the electron from the surface was measured by the TR-2PPE signal at 0.6 eV intermediate state energy. Additionally, Fig. 4.46 shows a fit curve with the underlying fit-model (line). The temporal shift of the peak against t_0, the rise, and also the very early decay of the signal were all fitted by means of optical Bloch equations for a two level system representing the initial ground and the intermediate excited state. This model is analogous to the one discussed in detail in Ref. [50]. With values for the parameters taken from experiment this model predicts a mono-exponential decay. The photoemission step was taken into account by the convolution of the intermediate state population with the probe pulse [6]. As the decay was non-exponential, this simple model could not fit the decay at longer times. Since, energy relaxation was negligible the decay must be ascribed to the escape of electrons from the detection depth of 2PPE.

Rego et al. have carried out combined DFT and quantum dynamical calculations on this system [7] to investigate the interfacial electron transfer dynamics [175]. These authors have reported that the charge is localized on the Ti^{4+} surface ions next to the catechol at very early times followed by an anisotropic delocalization of the charge with differences in time constants up to an order of magnitude

[6] The autocorrelation of the probe pulse was measured prior to the experiment on a Cu(111) sample.

[7] In the calculations of Rego et al. electron transfer was assumed to start from the excited LUMO state of catechol.

depending on the crystal direction. The proposed localization of the charge at early times is supported by a comparison between the linear absorption spectrum of a molecular Ti:catechol complex [176] and the absorption spectrum of the anatase TiO_2 catechol system [174]. The spectra suggest that the charge transfer complex formed in the latter system is similar to that in the molecular compound. Measurements on the anatase TiO_2 catechol systems suggest a bidentate bonding between catechol and TiO_2 [171]. Thus, the surface complex may comprise more than one Ti atom. Calculations suggest, however, that the electron is primarily located on just one Ti atom belonging to the surface complex just after excitation [172, 175, 177].

Stier et al. have carried out non adiabatic molecular dynamics simulations for a similar system [177]. They have reported that the electrons are localized to a high degree just after arrival in the TiO_2 [8]. The subsequent delocalization from near-surface states to bulk-like states is non-exponential with a dominant time constant of 100 fs [178].

Assuming a similar behavior of the system under investigation, the calculated dynamics combined with the restricted information-depth of our experiment should lead to a highly non-exponential evolution of the 2PPE signal at early times. Once the delocalization process is finished, recombination with the hole left behind on the catechol takes place on a longer time scale.

Therefore, the Bloch model was combined with a two-level rate model (inset of Fig. 4.46). The latter was appropriate since it turned out that the coherence decayed very fast (< 5 fs). Photoionization can be described classically for times where the coherence has decayed prior to the arrival of the probe pulse [51]. The contributions of the individual levels to the 2PPE signal were weighted by σ_i factors, thereby modeling Lambert-Beer's law and also the escape depth of photoelectrons. Thus, the parameter γ_i and σ_i model the anisotropic delocalization of electrons and the detection probability, respectively, in a phenomenological way. The time constants $\left(\tau_i = \frac{1}{\gamma_i}\right)$ resulting from the fit-model depicted in the inset of Fig. 4.46 are: $\tau_1 < 5$ fs, $\tau_2 = 85$ fs, $\tau_3 = 900$ fs, with weight factors: $\sigma_1 = 1.07$, $\sigma_2 = 0.05$, $\sigma_1 = 0.02$.

The method of choice for investigating the escape of electrons from the surface is photo-generation of electrons at the surface via suitable adsorbates, here the catechol:TiO_2 charge transfer complex. Since energy relaxation of the electrons is sufficiently slow in the present system it appears particularly suited for a comparison between the measured time-dependent escape (Fig. 4.46) and theoretical models in the spirit of Ref. [177, 178].

[8] Stier et al. used the excited state of alizarin as injecting level.

The discussed dynamics are believed to be independent of the specific nature of the electron donor, here the catechol molecule. Replacing the catechol with a molecule where the neutral excited state is the electron donor, e.g. a substituted perylene, introduces another time constant into the system. This time constant is the injection time of the molecule, i.e. the time it takes for the electron to leave the molecule. Hence, in such a case of a finite electron transfer time the escape dynamics measured above with catechol is a sequel to the electron transfer of the electron from the molecule. In terms of the fit-model used in this section, an additional rate enters the model. It is the rate by which the escape model is fed by the electron injection process.

The combined Bloch model described above is rather CPU-intensive when used in a fitting routine. Essentially, this is because the pump pulse enters the Bloch model and the solution of the combined model has to be convoluted with the probe pulse. In a pure rate model the convolution drops out of the rate equations and the crosscorrelation between pump and probe pulse can be taken as the generating term. It has been already mentioned that the main effect of the Bloch model with the restrictions given in Sec. 2.4.1 is a shift in t_0 that depends on the dephasing-time. Because, the fitted lifetime from the Bloch model was below 2 fs the maximum dephasing-time is 4 fs. However, the fitted dephasing-time was also below 2 fs. Hence, a pure rate model was taken to fit the dynamics in the catechol system and revealed essentially the same result. The model for the catechol system is shown in Fig. 4.47(a). The model for describing the TR-2PPE signal for the perylene derivatives with short anchor groups is illustrated in Fig. 4.47(b). The only difference is the additional rate γ_1 which accounts for the injection time. In the next section

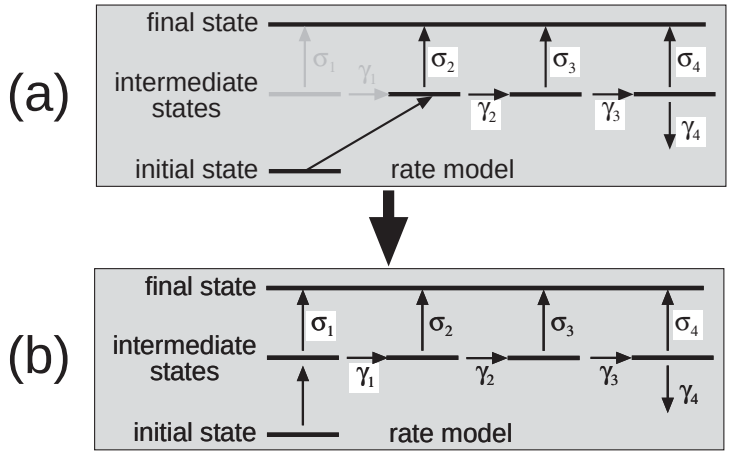

Figure 4.47: The rate model for the catechol system (a) and the rate model for the perylene derivatives with short anchor groups (b).

the latter model is used to extract the injection times of the different perylene chromophores with short spacer groups from the measured TR-2PPE signals.

4.3.4 Injection dynamics of perylene derivatives with short anchor groups attached to TiO_2

Five different perylene derivatives were available, three were equipped with a carboxylic acid group and two with a phosphonic acid group. The chemical structures are given in Fig. 2.10. The preparation of the TiO_2 rutile crystals and the coating with the molecules is described in Sec. 3.4.2 and 3.4.2.1. The parameters used for the different experiments are summarized in App. A.

A major prerequisite for applying the fit-model described in the previous section is that the electron distribution measured via 2PPE reveals the same time behavior as obtained from the catechol measurement. The distribution of injected electrons has been predicted to be controlled by the Franck-Condon progression of the Pe→Pe^+ transition and by the density of unoccupied electronic states in the solid [24]. TR-2PPE is the only experimental tool to verify at the same time the validity of the wide band limit condition [24] and to measure the corresponding electron transfer time which is in this unique case controlled by the strength of the electronic coupling and the density of unoccupied electronic states. The measured energy distribution of the injected electrons shows directly whether the whole Franck-Condon spectrum is accommodated in the conduction band, i.e. the validity of the wide band limit. The energy relaxation of the injected electrons appears to be sufficiently slow in TiO_2 to obtain the latter energy distribution of the injected electrons. To verify this important point 2PPE energy spectra were measured at different delay times (Fig. 4.48). For comparison the spectra of electrons injected by the direct optical charge transfer transition of catechol are shown as well. The stationary background was subtracted and the spectra are normalized. The signal at 200 fs was to small for Pe'-COOH and Pe'-CH=CH-COOH to be shown.

Obviously, the shape of the spectra of all the perylene derivatives stayed constant even for delay times where the molecular electron transfer was completed and most of the signal was expected to originate from electrons injected much earlier into the TiO_2 surface region.

The time dependent 2PPE spectra are explained as follows. At zero delay time most of the signal is expected to originate from electrons emitted from the excited state of the molecule. The energy distribution is a superposition of

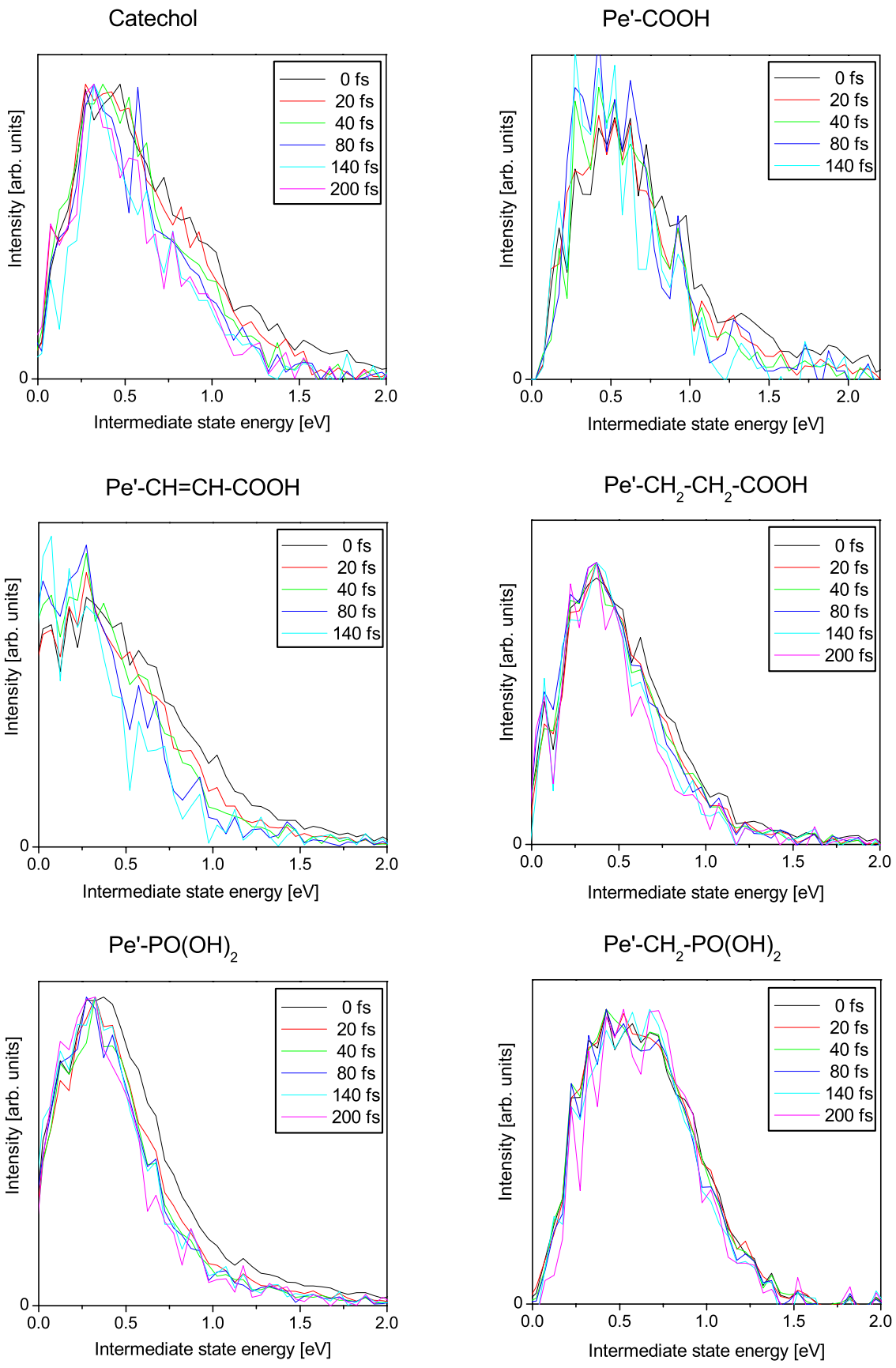

Figure 4.48: 2PPE spectra at different delay times for the perylene derivatives and catechol. The stationary background was subtracted and the spectra are normalized.

the Franck-Condon broadening in the excitation step and the Franck-Condon broadening of the photoinjection step [24]. For longer delay times part of the signal is expected to originate from electrons emitted from states in the surface region of TiO_2 and the spectra for delay times of 200 fs [9] are expected to originate nearly completely from electrons already injected into the TiO_2 substrate. The fact that the shape of the spectra remains the same can be explained by the assumption that energy relaxation is sufficiently slow in TiO_2. The negligible energy relaxation for the injected electrons in TiO_2 that was already observed in the catechol experiment leads to the conservation of the 2PPE spectrum at later delay times. Thus, the assumption that the evolution of the 2PPE signal originating from electrons injected from the excited state of perylene into empty states in the surface region of TiO_2 is comparable to that observed in the catechol experiment appears to be reasonable. The remarkable feature of the spectra in Fig. 4.48 is the first experimental proof for the theoretical predicted accommodation of the whole Franck-Condon envelope in the electronic acceptor states of the conduction band [24]. These spectra give the first direct experimental proof for the hitherto postulated validity of the wide band limit for the perylene:TiO_2 system. The electronic spectra in Fig. 4.48 represent the whole Marcus curve realized at once in the case of the wide band limit.

The extended fit model discussed in the previous section is applicable to fit the TR-2PPE signals also for perylene derivatives with short anchor groups. The fit model illustrated in Fig. 4.47 (b) was applied to fit transient 2PPE traces for the different perylene derivatives. The transient signals were recorded at the energetic positions of the excited states given in Tab. 4.1.3.1 in an energy window of 200 meV width. For Pe'-COOH, Pe'-CH=CH-COOH and Pe'-$PO(OH)_2$ t_0 and also the width of the crosscorrelation could be determined from a time trace measured around 2.5 eV kinetic energy. Crosscorrelations were also measured on a Cu (111) sample for comparison. For Pe'-CH_2-CH_2-COOH and Pe'-CH_2-$PO(OH)_2$, t_0 and the width of the crosscorrelation were measured on a Cu (111) sample. For the samples where it was possible to extract t_0 and the width of the CC directly from the measurement both values were fixed in the fitting procedure. For Pe'-CH_2-CH_2-COOH and Pe'-CH_2-$PO(OH)_2$ a 5 fs uncertainty was taken into account for the position of t_0. The free parameters in the fit were firstly the injection time τ_1 and secondly the weight factors σ_1 and σ_4. The results of the fits are given in table 4.3.4. It was necessary to allow a variation of the weight factor σ_4 to account for the variations in the

[9] 140 fs for the fast injecting molecules Pe'-COOH and Pe'-CH=CH-COOH.

Compound name	τ_1 fs	τ_2 fs	τ_3 fs	τ_4 fs	σ_1	σ_2	σ_3	σ_4
Catechol	.1	1.3	85.3	946.6	0	1.07	0.051	0.019
Pe'-COOH	8.4	"	"	"	0.010	"	"	0.012
Pe'-CH=CH-COOH	13.5	"	"	"	0.009	"	"	0.013
Pe'-CH=CH-COOH 2'nd	11.5	"	"	"	0.013	"	"	0.005
Pe'-CH_2-CH_2-COOH	47.2	"	"	"	0.017	"	"	0.007
Pe'-$PO(OH)_2$	23.5	"	"	"	0.005	"	"	0.009
Pe'-CH_2-$PO(OH)_2$	35.9	"	"	"	0.015	"	"	0.006

Table 4.2: Fit Parameter for the perylene derivatives with short anchor groups.

amplitude of the signal at long delay times. These variations may stem from sample inhomogeneities as well as differences in the coverage with the molecules. Nevertheless, the variations of σ_4 stayed within close bounds.
The difference in the injection time between identically prepared samples was 15% and the high energy part of the spectra was nearly identical. An extensive test of the reproducibility of the experiments with a large number of identically prepared samples was not possible because of the time consuming preparation procedure.
The injection times τ_1 are in overall good agreement with the ones derived from transient absorption spectroscopy on colloidal systems [64]. A comparison between the injection times obtained from TR-2PPE measurements and from transient absorption spectroscopy is given in table 4.3.4. The exact knowledge of

Compound name	TR-2PPE injection time [fs]	Trans Abs injection time [fs]
Pe'-COOH	8.4	13
Pe'-CH=CH-COOH	13.5	10
Pe'-CH_2-CH_2-COOH	47.2	57
Pe'-$PO(OH)_2$	23.5	28
Pe'-CH_2-$PO(OH)_2$	35.9	63

Table 4.3: Comparison between electron injection times measured via TR-2PPE and transient cation absorption spectroscopy taken from Ref. [64].

t_0 turned out to be of great importance especially for the short injection times.

Fits with t_0 as a fit parameter tended to converge badly with unrealistic values for t_0 and the injection time. This may be one reason why the two injection times for the two molecules where it was not possible to extract t_0 directly from the measurement showed a larger deviation from the injection times measured with transient absorption. Another reason is that once τ_1 is of the same order of magnitude as τ_3, τ_1 depends strongly on the value of σ_1 and the fit converges badly. The fitted time traces are shown in Fig. 4.49. While the model fits the measured data quite well at early times, at later times a significant deviation from the measured values is observed. However, these deviations show that the applied model is too simple to account for the complicated escape dynamics of the electrons from the surface region of TiO_2 discussed in Sec. 4.3.3. In addition, it was assumed here that the target states in the surface region of TiO_2 for the electrons injected from the excited state of perylene are the same as for the direct charge transfer in the catechol:TiO_2 system. This assumption may not hold because these states may be influenced by the binding geometries of the different anchor groups of catechol and the perylene derivatives. Such effects may affect some details, but the overall experimental verification of the theoretical injection model for the case of the wide band limit [24, 23, 179] by the TR-2PPE data presented in this work is already very satisfactory.

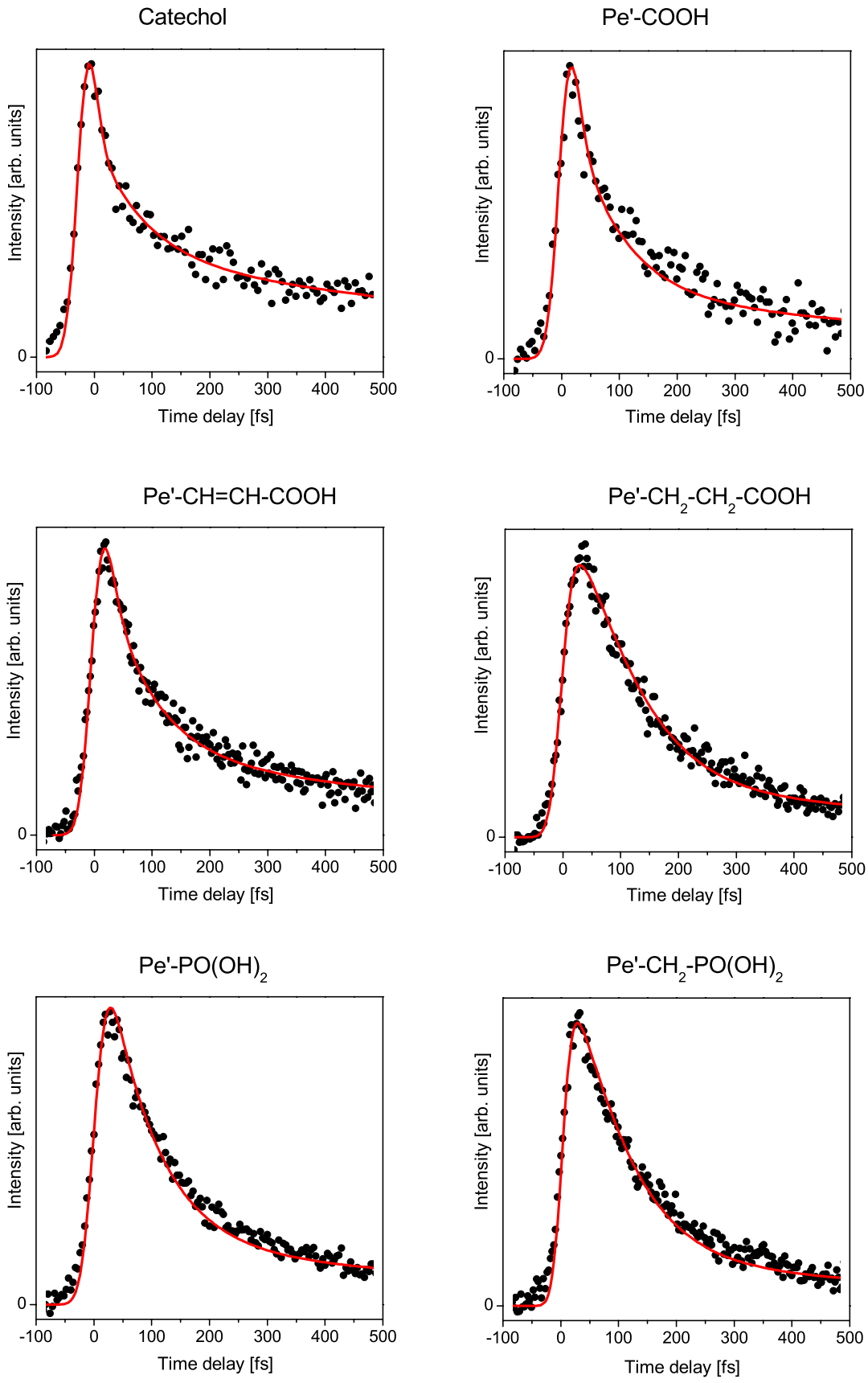

Figure 4.49: Time dependent 2PPE signal measured at the excited state energy for the different perylene derivatives (black dots). Fit with the model depicted in Fig. 4.47 (b) (red line).